



ORIGINAL ARTICLE

Synthesis and study of the trypanocidal activity of catechol-containing 3-arylcoumarins, inclusion in β -cyclodextrin complexes and combination with benznidazole



Josué Pozo-Martínez^{a,b}, Francisco Salgado^{a,c}, Ana Liempi^{a,b}, Ulrike Kemmerling^b, Raúl Mera-Adasme^d, Claudio Olea-Azar^{a,*}, Mauricio Moncada-Basualto^{a,b}, Fernanda Borges^e, Eugenio Uriarte^f, Maria João Matos^{e,f,*}

^a Laboratorio de Radicales Libres y Antioxidantes, Facultad de Ciencias Químicas y Farmacéuticas, Universidad de Chile, Chile

^b Laboratorio de Mecanismos de Infección Parasitaria, Facultad de Medicina, Universidad de Chile, Chile

^c Departamento de Ciencias Químicas, Facultad de Ciencias Exactas, Universidad Andrés Bello, Quillota 980 Viña del Mar, Chile

^d Departamento de Ciencia del Ambiente, Facultad de Química y biología, Universidad de Santiago de Chile, Chile

^e CIQUP/Departamento de Química e Bioquímica, Faculdade de Ciências, Universidade do Porto, 4169-007 Porto, Portugal

^f Departamento de Química Orgánica, Faculdade de Farmacia, Universidade de Santiago de Compostela, 15782 Santiago de Compostela, Spain

Received 7 October 2021; accepted 13 December 2021

Available online 16 December 2021

KEYWORDS

Chagas disease;
Trypanosoma cruzi;
3-Arylcoumarins;
Inclusion complex;
Benznidazole synergy

Abstract American trypanosomiasis or Chagas disease is caused by the protozoan parasite *Trypanosoma cruzi*, and is considered a neglected disease, being an important problem for public health. Benznidazole (BZN) is the drug used to treat the disease. However, it has limited efficacy and adverse side effects. Therefore, the development of new therapeutic alternatives is necessary. In this work, the trypanocidal activity and cytotoxicity of a series of catechol-containing 3-arylcoumarins, their combination with BZN, and the inclusion in β -cyclodextrins (β -CDs), were evaluated. The results obtained showed that the entire series has moderate trypanocidal activity on the trypomastigote form of the parasite, being the 3-(4'-bromophenyl)-6,7-dihydroxycoumarin (**8**) the most active compound ($IC_{50} = 34 \mu M$) and the most cytotoxic in Vero cells ($IC_{50} = 162 \mu M$) as well. By forming the inclusion complex **8**- β -CDs, the trypanocidal activity and cytotoxicity

* Corresponding authors.

E-mail addresses: colea@uchile.cl (C. Olea-Azar), mariajoao.correia-pinto@usc.es, maria.matos@fc.up.pt (M.J. Matos).

Peer review under responsibility of King Saud University.



decreased. In addition, the formation of inclusion complexes increased the solubility. The possible mechanism of action of **8** was evaluated and proved to be through the generation of oxidative stress. The combination with BZN presented a synergistic effect on the trypanocidal activity, reducing the necessary dose of BZN. The presence of a catechol in the studied scaffold seems to modulate the trypanocidal activity, and the combination of drugs proved to be a promising alternative strategy for treating the disease.

© 2021 The Authors. Published by Elsevier B.V. on behalf of King Saud University. This is an open access article under the CC BY license (<http://creativecommons.org/licenses/by/4.0/>).

1. Introduction

Chagas disease or American trypanosomiasis is caused by the protozoan parasite *Trypanosoma cruzi* (*T. cruzi*) and is endemic in Latin America (Souza et al., 1998). Chagas disease is considered one of the world most neglected and emerging tropical diseases. The *T. cruzi* parasite has a complex life cycle with three cell forms: trypomastigote and amastigote present in the mammal, and epimastigote in the vector (Estani and Segura, 2017).

Two drugs, nifurtimox (NFX) and benznidazole (BZN), developed 50 years ago, are used to treat the disease. They are effective in the acute phase of the disease while their effect decreases in the chronic phase. However, they present severe secondary effects (Chatelain, 2014; Forsyth et al., 2016). Therefore, it is necessary to develop new drugs that are more effective and less toxic. In this context, coumarin derivatives have been proposed as possible trypanocidal agents.

Based on this, our group has synthesized different series of coumarins with various substituents linked to their scaffold under a rational design. Their activity may be related to the inhibition of enzymes and/or the generation of oxidative stress (Matos et al., 2013; Moncada-Basualto et al., 2019; Pérez-Cruz et al., 2013; Robledo-O’Ryan et al., 2017; Salgado et al., 2021). Our group previously synthesized a series of 3-amidocoumarins, and the influence of the substituents on the trypanocidal activity and antioxidant capacity was evaluated (Moncada-Basualto et al., 2018). Particularly, the presence of a hydroxyl group at position 4 proved to increase the antioxidant capacity, while decreasing the trypanocidal activity. Likewise, the presence of an amide at position 3 of the coumarin modulates the trypanocidal activity. In addition, a possible mechanism of action by the generation of oxidative stress in the parasite, was determined. Therefore, this type of compounds emerged as promising trypanocidal agents. However, the series turned out to be slightly cytotoxic against mammalian cells, but variations on the scaffold may improve the selective trypanocidal activity.

Looking for improved properties, our group also synthesized a new series of hydroxy-3-aryl coumarins, and evaluated the trypanocidal activity in both epimastigote and trypomastigote forms of *T. cruzi* (Robledo-O’Ryan et al., 2017). This study showed that the presence of hydroxyl substituents decreases the cytotoxicity in the mammalian cell line RAW 264.7. Also, the presence of a catechol improves the trypanocidal activity. Furthermore, the lipophilicity modulates the trypanocidal activity, possibly by increasing cell membrane permeability. The mechanism of trypanocidal action proposed for that series is through the generation of oxidative stress. Therefore, the study of compounds with a structural similarity

to those studied previously, and with modification in the position of a catechol, and the substituents in the aryl at position 3, may lead to the discovery of a promising new group of trypanocidal agents.

Another strategy used in the search for new treatments for diseases caused by protozoan parasites is combining traditional drugs with new bioactive compounds to enhance the therapeutic activity and reduce the adverse effects of conventional drugs (Seguel et al., 2016; Ulrich-Merzenich, 2014). Therefore, the combination of antioxidants with BZN has been studied for treatment of the acute phase of Chagas disease, since there is a high proliferation of parasites and inflammatory response that aggravates the generation of reactive oxygen and nitrogen species (ROS and RNS) (Castanheira et al., 2018; Goes et al., 2016). Conventional drugs –BZN and NFX– being nitroheterocyclic compounds, increase nitrosative and oxidative stress. This oxidative environment, associated with the intracellular multiplication of *T. cruzi*, leads to the destruction of the host tissues, thus contributing to the etiopathogenesis of the disease. Moreover, the trypanocidal mechanism of BZN also involves: i) covalent modification of macromolecules through the formation of cytotoxic metabolites such as glyoxal; ii) increased phagocytosis of *T. cruzi* by host cells with consequent production of cytokines, and iii) inhibition of NADH-fumarate reductase in the parasite (de Alcántara et al., 2015; Hall et al., 2011; Wilkinson et al., 2008), where the former mechanisms are responsible for the adverse effects in the host. Thus, the possibility of reducing the dose of BZN in combination with new promising compounds such those proposed herein seems to be an attractive strategy in the search for treatments for chronic patients. In this context, combinations of BZN with ascorbic acid have been studied in *in vivo* murine models, demonstrating that the combination of both compounds reduces parasitemia, intracellular ROS, and lipid peroxidation in cardiac tissue, more effectively than each compound *per se* (Pelizzaro-Rocha et al., 2010; Providello et al., 2018). In addition, BZN and parthenolide have a synergistic effect against the *T. cruzi* epimastigote, reducing the IC₅₀ of BZN by 23 times (Pelizzaro-Rocha et al., 2010). Therefore, the study of the combination of catechol-containing 3-aryl coumarins with BZN could be a double strategy to search for active trypanocidal therapies, with less side effects.

Unfortunately, many lipophilic organic compounds, including coumarins, do not reach their intracellular targets due to low solubility in an aqueous medium, and pH and temperature conditions. The formation of inclusion complexes with cyclodextrins (CDs) may surpass these handicaps. CDs may increase the solubility, while preserving the bioactive properties of the compounds in physiological media (Chen et al., 2013). We previously demonstrated that both the try-

panocidal activity and bioavailability of inclusion complexes of 3-amidocoumarins with mono-6-amino-6-deoxy- β -CDs increased, comparing to the free compounds (Moncada-Basualto et al., 2019). Also, a variation of the parasites mitochondrial membrane potential of the inclusion complexes was observed, compared to the free compounds.

In this work, a series of catechol-containing 3-arylcoumarins (homo and heteroaryl) was synthesized, with the catechol group in different positions of the coumarin scaffold. The aryl group should increase the lipophilicity of the compounds, while the catechol group should modulate the trypanocidal activity, particularly in combination with BZN. Then, the most effective compound in the series was included in β -CD, and its cytotoxicity, bioavailability, and possible mechanisms of action, were evaluated.

2. Experimental section

2.1. Chemistry

2.1.1. General information

All reagents were purchased from Sigma-Aldrich and used without further purification. All solvents were commercially available grade. All reactions were carried out under argon atmosphere, unless otherwise mentioned. Reaction mixtures were purified by flash column chromatography using Silica Gel high purity grade (Merck grade 9385 pore size 60 Å, 230–400 mesh particle size). Reaction mixtures were analyzed by analytical thin-layer chromatography (TLC) using plates precoated with silica gel (Merck 60 F254, 0.25 mm). Visualization was accomplished with UV light (254 nm), ninhydrin or potassium permanganate (KMnO₄). ¹H NMR and ¹³C NMR spectra were recorded on a Bruker AMX spectrometer at 250 and 62.90 MHz in the stated solvent (DMSO-*d*₆) using tetramethylsilane (TMS) as an internal standard. Chemical shifts were reported in parts per million (ppm) on the δ scale from an internal standard (NMR descriptions: s, singlet; d, doublet; dd, double doublet; t, triplet; m, multiplet). Mass spectroscopy was performed using a Hewlett-Packard 5988A spectrometer. This system is an automated service utilizing electron impact (EI) ionization.

2.2. Synthetic methodology

Synthetic methodology for the acetoxyated precursors.

Acetoxy-3-arylcoumarins were synthesized under anhydrous conditions, using material previously dried at 60 °C for at least 12 h and at 300 °C during few minutes immediately before use. A solution containing anhydrous CH₃CO₂K (2.94 mmol), ary-lacetic or heteroarylacetic acid (1.67 mmol), and the corresponding hydroxysalicylaldehyde (1.67 mmol), in Ac₂O (1.2 mL), was refluxed for 16 h. The reaction mixture was cooled, neutralized with 10% aqueous NaHCO₃, and extracted with EtOAc (3 × 30 mL). The organic layers were combined, washed with distilled water, dried (anhydrous Na₂SO₄), and evaporated under reduced pressure. The product was purified by recrystallization in EtOH and dried to afford the desired compound.

Synthetic methodology for the hydroxyl derivatives 1–11. Compounds 1–11 were obtained by hydrolysis of their acetoxyated counterparts, respectively. The appropriate acetoxy-

lated coumarin, mixed with 2 N aqueous HCl and MeOH, was refluxed during 3 h. The resulting reaction mixture was cooled in an ice-bath and the reaction product, obtained as solid, was filtered, washed with cold distilled water, and dried under vacuum to afford the desired compound.

3-(3',4'-Dihydroxyphenyl)coumarin (1). (Erk, Bulut, & Göçen, 2000)

3-(3',4'-Dihydroxyphenyl)-6-hydroxycoumarin (2). (Fais et al., 2018)

3-(3',4'-Dihydroxyphenyl)-6-methylcoumarin (3). (Matos et al., 2013)

3-(3',4'-Dihydroxyphenyl)-8-methylcoumarin (4). (Matos et al., 2013)

6,7-Dihydroxy-3-(2'-hydroxyphenyl)coumarin (5). Yield: 80%. Rf (Hexane/Ethyl Acetate 5:5): 0.05. Mp: 265–267 °C. ¹H NMR (DMSO-*d*₆) δ (ppm), *J* (Hz): 6.76–6.88 (m, 3H, H-5, H-8, H-5'), 6.97–7.03 (m, 1H, H-4'), 7.18–7.22 (m, 2H, H-2', H-3'), 7.82 (s, 1H, H-4), 9.40 (s, 1H, OH), 9.46 (s, 1H, OH). ¹³C NMR (DMSO-*d*₆) δ (ppm): 102.43, 111.41, 112.41, 115.75, 118.77, 123.03, 129.32, 131.07, 142.54, 143.00, 148.15, 150.14, 155.20, 155.55, 166.67. MS *m/z* (%): 392.1 (16), 391.1 (29), 390.0 (100).

6,7-Dihydroxy-3-(3'-hydroxyphenyl)coumarin (6). (Juvonen et al., 2020)

3-(2'-Bromophenyl)-6,7-dihydroxycoumarin (7). Yield: 86 Rf (Hexane/Ethyl Acetate 5:5): 0.08. Mp: 248–250 °C. ¹H NMR (DMSO-*d*₆) δ (ppm), *J* (Hz): 6.67 (s, 1H, H-8), 7.33 (s, 1H, H-5), 7.38–7.42 (m, 3H, H-4', H-5', H-6'), 7.65–7.68 (m, 1H, H-3'), 7.86 (s, 1H, H-4), 9.46 (s, 1H, OH), 10.29 (s, 1H, OH). ¹³C NMR (DMSO-*d*₆) δ (ppm): 102.58, 110.90, 112.60, 123.56, 123.66, 127.82, 130.19, 130.74, 132.00, 136.88, 143.22, 150.83, 153.87, 156.70, 164.60. MS *m/z* (%): 385.1 (12), 384.2 (30), 383.1 (100).

3-(3'-Bromophenyl)-6,7-dihydroxycoumarin (8). Yield: 86%. Rf (Hexane/Ethyl Acetate 5:5): 0.06. Mp: 255–257 °C. ¹H NMR (DMSO-*d*₆) δ (ppm), *J* (Hz): 6.73–6.76 (m, 1H, H-8), 7.02–7.05 (m, 1H, H-5), 7.31–7.49 (m, 1H, H-6'), 7.50 (d, 1H, H-5', *J* = 8.5), 7.66 (d, 1H, H-4', *J* = 8.5), 7.86–7.89 (m, 1H, H-2'), 8.16 (s, 1H, H-4), 9.50 (s, 1H, OH), 10.31 (s, 1H, OH). ¹³C NMR (DMSO-*d*₆) δ (ppm): 102.34, 111.48, 121.51, 127.36, 130.36, 130.65, 130.81, 130.85, 137.77, 139.82, 142.12, 143.24, 148.38, 151.07, 165.97. MS *m/z* (%): 335.0 (16), 333.9 (99), 332.9 (14), 332.0 (100).

3-(4'-Bromothiophen-2'-yl)-6,7-dihydroxycoumarin (9). Yield: 74%. Rf (Hexane/Ethyl Acetate 8:2): 0.07. Mp: 286–288 °C. ¹H NMR (DMSO-*d*₆) δ (ppm), *J* (Hz): 6.78 (s, 2H, H-5, H-7), 7.01 (s, 1H, H-4'), 7.73 (s, 1H, H-2'), 8.60 (s, 1H, H-4), 9.66 (s, 1H, OH), 10.46 (s, 1H, OH). ¹³C NMR (DMSO-*d*₆) δ (ppm): 103.6, 109.8, 114.2, 116.8, 123.1, 126.8, 129.1, 137.9, 145.8, 146.1, 150.1, 162.3. MS *m/z* (%): 341.0 (14), 339.9 (89), 339.3 (9), 337.9 (89).

6,7-Dihydroxy-3-(thiophen-2'-yl)coumarin (10). Yield: 86%. Rf (Hexane/Ethyl Acetate 5:5): 0.06. Mp: 238–239 °C. ¹H NMR (DMSO-*d*₆) δ (ppm), *J* (Hz): 6.77 (s, 1H, H-5), 7.04 (s, 1H, H-8), 7.09 (t, 1H, H-4', *J* = 4.0), 7.54 (dd, 1H, H-3', *J* = 4.0, 1.0), 7.72 (dd, 1H, H-5', *J* = 4.0, 1.0), 8.40 (s, 1H, H-4), 9.48 (s, 1H, OH), 10.28 (s, 1H, OH). ¹³C NMR (DMSO-*d*₆) δ (ppm): 102.42, 111.39, 112.24, 125.27, 127.26, 127.55, 128.84, 136.24, 137.16, 142.08, 143.51, 150.73, 163.74. MS *m/z* (%): 261.1 (16), 260.1 (100).

6,7-Dihydroxy-3-(thiophen-3'-yl)coumarin (11). Yield: 84%. Rf (Hexane/Ethyl Acetate 5:5): 0.06. Mp: 235–236 °C. ¹H

NMR (DMSO-*d*₆) δ (ppm), J (Hz): 6.74 (s, 1H, H-5), 7.01 (s, 1H, H-8), 7.58–7.64 (m, 2H, H-3', H-4'), 8.10 (s, 1H, H-2'), 8.31 (s, 1H, H-4), 9.48 (s, 1H, OH), 10.24 (s, 1H, OH). ¹³C NMR (DMSO-*d*₆) δ (ppm): 102.34, 111.42, 112.25, 112.27, 124.10, 126.08, 126.85, 135.33, 135.86, 139.12, 143.28, 150.52, 160.04. MS m/z (%): 261.1 (16), 260.1 (100).

2.3. Oxygen radical antioxidant Capacity-fluorescein (ORAC-FL)

Antioxidant capacity was determined using the ORAC-fluorescence methodology (ORAC-FL) (Moncada-Basualto et al., 2018; K. Pérez-Cruz et al., 2018; Robledo-O'Ryan et al., 2017). The analysis was performed using a 96-well white polystyrene plate reader (EnSpire multimode PerkinElmer, Waltham, MA, USA). The reaction was carried out in phosphate buffer (75 mM, pH 7.4). The compound solutions were prepared in dimethyl sulfoxide (DMSO, 0.1 to 2.3 μ M), homogenized and incubated at 37 °C, for 5 min, with 150 mL of fluorescein solution (40 nM, final concentration). Then, 25 mL of 2,2-azobis(2-methylpropionamidine) dihydrochloride (Sigma-Aldrich 97%, St. Louis, MO, USA) 18 mmol L⁻¹ were added, and the fluorescence was registered (excitation wavelength of 485/20 nm and emission filter of 528/20 nm) at a constant temperature of 37 °C, in a Synergy HT multi-detection microplate reader (Bio-Tek Instruments, Winooski, VT, USA), every minute for 2 h. A blank with FL and AAPH, using dimethyl sulfoxide instead of the antioxidant solution, was used in each assay. Five calibration solutions using Trolox (0.1 to 10 μ M) were also used in each assay. The inhibitor capacity was expressed as ORAC-FL values, and it was quantified by the integration of area under the curve (AUC_{NET}). All reaction mixtures were prepared in triplicate, and at least three independent assays were performed for each sample. The area under the fluorescence decay curve (AUC) was calculated integrating the fluorescence decay where F_0 is the initial fluorescence read at 0 min, and F is the fluorescence read at time. The AUC_{NET} corresponding to the sample was calculated by subtracting the AUC corresponding to the blank. Data processing was performed using Origin Pro 8.5 SR2 (Origin Lab Corporation, USA). The ORAC-FL indices were calculated according to the following equation (1):

$$\text{ORAC - FLindex} = \frac{(\text{AUC}_{\text{AH}} - \text{AUC}_{\text{CONTROL}})}{(\text{AUC}_{\text{AH}} - \text{AUC}_{\text{CONTROL}})} \times \frac{[\text{TROLOX}]}{[\text{AH}]} \quad (1)$$

2.4. Determination of the Fukui index

All Fukui-related calculations were performed with TURBO-MOLE v7.5.0 (Balasubramani et al., 2020). The optimization of the structures of the neutral compounds was carried out at the B97-3c GGA density-functional level (Brandenburg et al., 2018) which includes the triple-zeta def2-mTZVP basis set and the D3 dispersion correction (Grimme et al., 2010) with Becke-Jonhson damping (Grimme et al., 2011). The RI approximation (Eichkorn et al., 1997) was used to speed up calculations. The descriptors were evaluated through the condensed orbital approximation based on natural population analysis (NPA) charges (Reed et al., 1985). The radical Fukui

is the average corresponding to nucleophilic (f_k^-) and electrophilic (f_k^+) attack reactions (equations (2)):

$$f_k^0 = \frac{f_k^- + f_k^+}{2} \quad (2)$$

2.5. Inclusion complex formation

The complex was prepared by mixing a solution of the 3-arylcoumarins in DMSO with β -CD (Sigma-Aldrich, Inc., St. Louis, MO) solution, in water, in a 1:3 M ratio. The concentration of DMSO in the mixture did not exceed 10% by volume (Folch-Cano et al., 2011).

2.6. Determination of the association constant of the inclusion complex

The determination of the constant was carried out through fluorescence or absorbance intensity measurements of the 3-arylcoumarins. The spectra absorbance was recorded between 280 and 600 nm, and for the fluorescence, the spectra emission was recorded between 380 and 600 nm, at a fixed excitation wavelength between 300 and 350 nm. Association constant was obtained by the linear equation of Benesi-Hildebrand (3) (Ackermann, 1987; Tablet et al., 2012):

$$\frac{1}{(F - F_0)} = \frac{1}{(K_c(F_\infty - F_0)[\beta\text{CDs}]_0)} + \frac{1}{(F_\infty - F_0)} \quad (3)$$

F_∞ is the fluorescence of 3-arylcoumarin included in β -CDs, and F_0 represents the fluorescence of the free 3-arylcoumarin.

2.7. Determination of the inclusion geometry of the complexes by molecular modeling

Inclusion geometries were determined at the quantum-chemistry level by employing the modern GFN2-xTB (Bannwarth et al., 2019) semiempirical method and a dielectric continuum for modeling the water solvation. The xtb program v6.3.3 (Bannwarth et al., 2021) was employed for all calculations. The β -CD structure, each ligand, and two complexes per ligand (each in one of the two possible orientations) were optimized. A 3 ns Born-Oppenheimer molecular dynamics simulation was then performed on each optimized structure. From the last 500 ps of each simulation, snapshots were sampled every 0.1 ps. Each frame was taken to its nearest minimum by geometry optimization, and Gibbs free energies were obtained from Hessian matrix calculations, except for those with imaginary modes after optimization.

2.8. Determination of the inclusion complex of the complexes by nuclear magnetic resonance

Inclusion geometry was determined by ¹H NMR and COSY (correlated spectroscopy) in a Bruker Advance 400 equipment (Billerica, MA, USA), equipped with a 5 mm diameter wide band inverse probe of z gradient, operated at an operating frequency of 400.13 MHz (¹H). The samples were prepared using deuterated methanol (for BZN) and deuterated water (for β -CDs and inclusion complex) as solvents.

2.9. Biological studies

2.9.1. Cell culture

Green Monkey (*Cercopithecus aethiops*) renal fibroblast-like cells [Vero cells (ATCC®CCL-81)] were grown in RPMI medium supplemented with 5% fetal bovine serum (FBS) and antibiotics (penicillin–streptomycin) (Villalta and Kierszenbaum, 1982). The cells were grown at 37 °C, in a humidified atmosphere with 5% CO₂. The culture medium was replaced every 24–48 h. Cells were counted in a Neubauer chamber, previous to the experiments.

2.9.2. Parasite cultures and harvesting

Stock cultures of *T. cruzi* epimastigotes (Dm28 strain) were maintained in axenic conditions at 28 °C in monobasic Diamond's culture medium supplemented with 75 µM hemin, 5% fetal bovine serum (FBS), 100 µg.mL⁻¹ sodium penicillin and 100 µg.mL⁻¹ streptomycin (Jimenez et al., 2014). Infective extracellular trypomastigotes were obtained from infected Vero cells. Semiconfluent Vero cells were incubated with epimastigotes of *T. cruzi* harvested in the late stationary phase. Trypomastigotes also present in the culture invade Vero cells and replicate intracellularly as amastigotes. After 72 h, amastigotes transform back into trypomastigotes which lyse the host cells. Trypomastigotes were recovered in the supernatant by low-speed centrifugation (500 × g), counted in a Neubauer chamber, and used for the viability assay (Veas et al., 2020).

2.9.3. Trypanocidal and cytotoxicity activity

Trypomastigotes (10⁷ parasite/mL) or Vero cells (500 cells/mL) were incubated with the compounds or BZN, resuspend in DMSO in culture medium (0.025% v/v, final concentration), for 24 h. IC₅₀ values were obtained by the dose–response analysis, where parasites or Vero cells were incubated with different concentrations of BZN and 3-arylcoumarins (20, 50, 80, 100 and 200 µM). For combination experiments, parasites were exposed for 24 h to the compound with the best trypanocidal activity and BZN. For the study about the outcome of the coumarin–BZN combinations, a dose–matrix approach was performed, comparing the effect of the combination of 7 concentrations of the coumarin (5, 10, 20, 34, 50, 100 and 200 µM) and 7 concentrations of BZN (5, 10, 20, 50, 100 and 200 µM). The data was then analyzed using the free software Combenefit (Di Veroli et al., 2016). Bliss independence approach was used for the data analysis, assuming that both drugs have different mechanisms of action.

The effects of the compounds on trypomastigote and Vero cells viability were evaluated by tetrazolium salt reduction assay (MTT). Briefly, 10 mL of 5 mg.mL⁻¹ MTT (3[4,5-dimethylthiazol-2-yl]-2,5-diphenyltetrazolium bromide) dye and 0.22 mg.mL⁻¹ phenazine methosulphate (used as an electron carrier) were added to each well containing 10⁷ parasites or 5 × 10⁴ cells in 100 mL of RPMI 1640 medium, without phenol red. After incubating the parasites or cells for 4 h at 37 °C, the generated formazan crystals were dissolved in 100 mL of 10% (w/v) SDS in 0.01 M HCl. The plates were kept overnight at 37 °C, and the optical density (OD) was determined using a microplate reader (LabSystems Multiskan MS, Finland) at 570 nm. Under these conditions, the OD is directly propor-

tional to the viable number of cells in each well (Veas et al., 2020).

2.9.4. Effect on intracellular parasite

Vero cells were detached by trypsinization, sedimented, and resuspended in media containing 10% FBS. Then, 5 × 10⁴ cells were seeded into 24-well plates. The cells were allowed to adhere to the bottom of the wells for 4 h, and were then challenged with the parasites at a Vero cell:parasite ratio of 1:3 for 24 h, after which the supernatant was removed, and the cells were exposed to the coumarin with the best trypanocidal activity at the IC₅₀ concentration, BZN, and the best coumarin combination. For the morphological analysis, Vero cells were fixed in cold 90% methanol and washed with PBS, and incubated with 1 µg.mL⁻¹ 4,6-diamidino-2-phenylindole (DAPI) (Molecular Probes). Then, the sections were mounted in Vectashield (ScyTek ACA) and observed on an epifluorescence microscope (Motic BA 310; Hong Kong, China). The amastigotes were recognized by their morphology, including nuclear size and the presence of a kinetoplast, and analyzed with the MATLAB® software (Liempi et al., 2015). At least 300 cells were analyzed per condition.

2.9.5. Determination of parasite DNA by real-time PCR

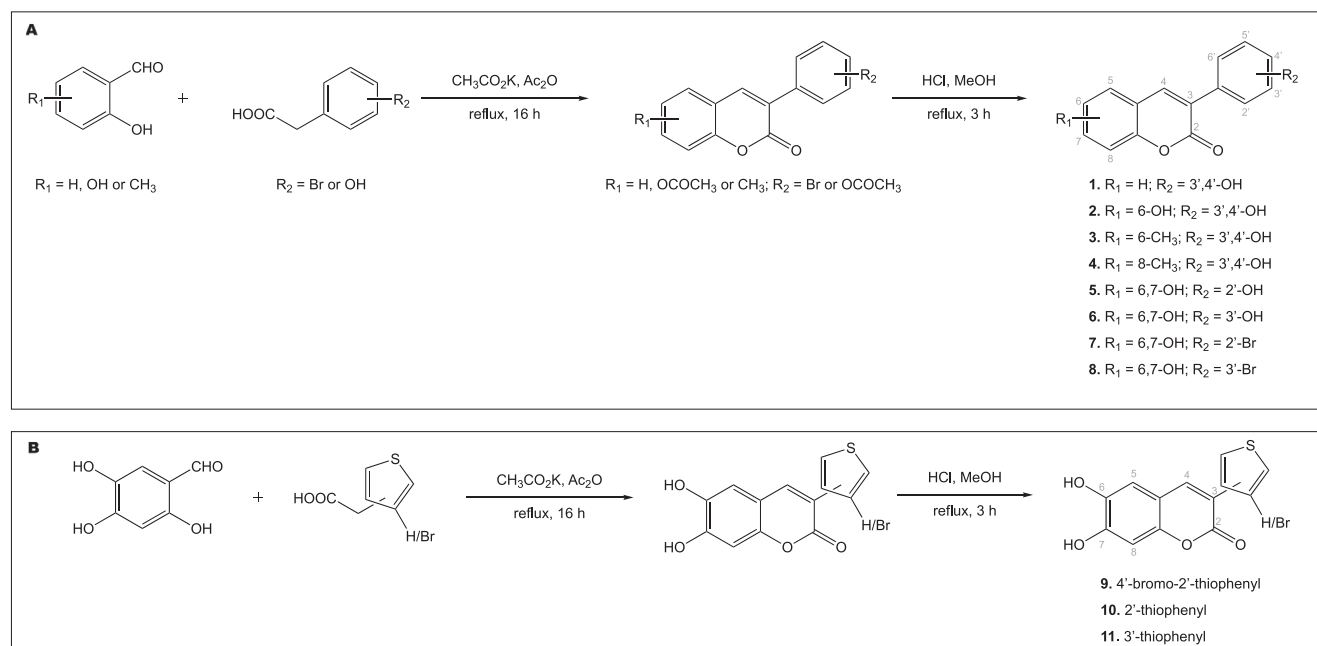
Genomic DNA was extracted from Vero cells with a Wizard Genomic DNA Purification Kit (Promega®, USA) according to the manufacturer's instructions. The resulting DNA was quantified with a µDrop Plate DNA quantification system in a Varioskan Flash Multimode Reader (Thermo Scientific, USA). For amplification of parasite DNA, two specific primer pairs were used. *T. cruzi* DNA detection, a 182 bp sequence of satellite DNA was amplified using the primers TCZ-F (5-GC TCTTGCCACAMGGTGC-3) and TCZ-R (5-CAAG CAGCGGATAGTTCAGG-3) (Veas et al., 2020). Each reaction mix contained 200 nM of each primer (forward and reverse), 1 ng of DNA, 12.5 µL. The amplification was performed in an ABI Prism 7300 sequence detector (Applied Biosystem®, USA). The cycling program was as follows: an initial incubation at 20 °C for 2 min, a denaturation step at 95 °C for 10 min, and 40 amplification cycles of 95 °C (15 s), 60 °C (15 s), and 72 °C (30 s). The final step was a dissociation stage that ranged from 60 to 95 °C (105 s). The relative quantification analysis of the results was expressed as an RQ (Duaso et al., 2012).

2.9.6. Detection of radical species in the parasite by ESR

As reported earlier, *T. cruzi* trypomastigotes (Dm28c) were grown at 37 °C in RPMI 1640 medium. The parasite concentration was 8 × 10⁷ cells corresponding to 1 mg of protein. ESR spectra were produced using parasite in trypomastigote stage, in a reaction medium containing 1 mM NADPH and 100 mM DMPO, in phosphate buffer (20 mM, pH 7.4). All experiments were performed after 10 min of incubation, at 37 °C, for 3-arylcoumarins (5 mM) with trypomastigote of *T. cruzi*, NADPH, and DMPO, in an aerobic environment.

2.9.7. Determination of the effect on mitochondrial membrane potential ($\Delta\psi_m$) in Dm28c trypomastigote of *T. Cruzi*

Mitochondrial membrane potential ($\Delta\psi_m$) was determined by the incorporation of the fluorescent probe tetramethylrho-



Scheme 1 Synthetic methodology for obtaining compounds **1–11** via Perkin-Oglialoro reaction. **A.** Synthesis of 3-homoarylcoumarins **1–8**. **B.** Synthesis of 3-heteroarylcoumarins **9–11**.

damine methyl ester (TMRM) (Moncada-Basualto et al., 2019). Trypomastigote of Dm28c strain (1×10^7 parasites/mL) were seeded in a 96-well plate, compounds, inclusion complex, and BZN were added to the concentration of IC_{50} . Then, carbonylcyanide-*m*-chlorophenylhydrazone (CCCP, 10 μM) was added and incubated at 37 °C, in humidified air and 5% CO_2 , for 3 h. Parasites were washed with phosphate-buffered saline (pH 7.4), and suspensions were incubated with TMRM (50 nM), for 15 min. The incorporation of the probe was determined by fluorescence measurements at an excitation wavelength of 550 nm and an emission of 590 nm. All the assays were performed in darkness.

2.10. Parallel artificial membrane permeability assays

Determination of permeability in the artificial membrane of coumarin derivatives was carried out according to the methodology described by Sierpe et al. (Sierpe et al., 2017). Donor plates contained 300 μL of the sample with a concentration of 0.5 mM (solubilized in 30% DMSO: 70% phosphate buffer pH 7.4). Compounds were quantified using spectrophotometry in a microplate spectrophotometer (Multiskan Spectrum, Thermo Electron Co.). PAMPA assay was performed in triplicate ($n = 3$), and experiments were carried out at least three times, data reported as means and their standard deviations from triplicate.

2.11. Statistical analysis

Statistical analysis was performed using Graph Pad Prism 4.03 (GraphPad Software, San Diego, California, USA). The data is expressed as mean \pm SD of three independent experiments. Statistical analysis was performed using one-way ANOVA

with Dunnett post-test. The data is considered statistically significant when $p < 0.05$.

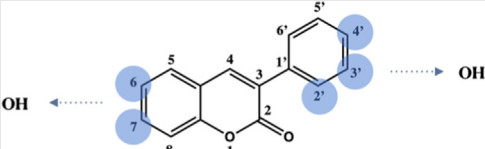
3. Results and discussion

3.1. Synthesis of 3-arylcoumarins

The described derivatives **1–11** were efficiently synthesized according to the protocol outlined in Scheme 1. 3-Arylcoumarins were obtained via Perkin – Oglialoro, a well-known two-steps condensation reaction. Firstly, *ortho*-hydroxybenzaldehydes and arylacetic acids react for 16 h, at reflux temperature, in the presence of potassium acetate ($\text{CH}_3\text{-CO}_2\text{K}$) and acetic anhydride (Ac_2O). Under these mild conditions, concomitant acetylation of the hydroxyl groups and

Table 1 ORAC-FL index of the studied 3-arylcoumarins **1–11**.

| Compound | ORAC-FL index |
|---------------|-----------------|
| 1 | 1.3 \pm 0.1 |
| 2 | 5.6 \pm 0.3 |
| 3 | 0.4 \pm 0.1 |
| 4 | 0.7 \pm 0.1 |
| 5 | 1.6 \pm 0.2 |
| 6 | 1.7 \pm 0.4 |
| 7 | 0.9 \pm 0.1 |
| 8 | 0.59 \pm 0.02 |
| 9 | 0.8 \pm 0.4 |
| 10 | 1.5 \pm 0.7 |
| 11 | 1.2 \pm 0.1 |
| Trolox | 1.0 |

Table 2 Fukui indices (f_k^0) of the studied 3-arylcoumarins 1–11.


| Compound | 1 | 2 | 3 | 4 | 5 | 6 | 7 | 8 | 9 | 10 | 11 |
|---------------|--------|--------|--------|--------|--------|--------|--------|--------|--------|--------|--------|
| f_k^0 Index | | | | | | | | | | | |
| O_4 | -0.060 | -0.052 | -0.058 | -0.059 | | | | | | | |
| O_3 | -0.046 | -0.040 | -0.044 | -0.049 | | -0.029 | | | | | |
| O_2 | | | | | -0.050 | | | | | | |
| O_6 | | -0.060 | | | | -0.040 | -0.055 | -0.047 | -0.037 | -0.038 | -0.036 |
| O_7 | | | | | -0.051 | -0.054 | -0.066 | -0.061 | -0.050 | -0.057 | -0.050 |
| C_4 | -0.111 | -0.102 | -0.109 | -0.113 | -0.102 | -0.096 | -0.094 | -0.093 | -0.094 | -0.101 | -0.102 |

closure of the pyrone ring occur, to afford the acetoxyated compounds in very high yields (90–95%). The appearance of the H-4 in the ^1H NMR of the final product corroborates the success of the reaction. The chemical shift of H-4 is between 7.8 and 8.6 ppm.

Secondly, the acetoxy derivatives are hydrolyzed in the presence of hydrochloric acid (HCl, 2 N) and methanol (MeOH), at reflux temperature, for 3 h, to yield the hydroxyl derivatives in very good yields (85–90%). The appearance of the peaks corresponding to the hydroxyl (broad singlets), and the disappearance of the peaks corresponding to the methyl group from the acetoxy substituent (big peak integrating for three protons) in the ^1H NMR of the final product, corroborate the success of the reaction. The chemical shift of the hydroxyl is between 9.40 and 10.35 ppm, and the chemical shift of the methyl is around 2.30 ppm.

3.2. Antioxidant capacity

The antioxidant capacity of the series of catechol-containing 3-arylcoumarins was determined by the ORAC-FL methodol-

ogy, using a fluorescent probe to scavenge oxygen-centered radicals (Table 1). Compounds 1, 2, 5, 6, and 11 presented higher antioxidant capacity than trolox, used as control. The high antioxidant capacity of the 3-(3',4'-dihydroxyphenyl)-6-hydroxycoumarin (2) is in concordance with our previous studies (Robledo-O'Ryan et al., 2017), which determined that the presence of a hydroxyl group at position 6 of the 3-phenylcoumarin increases the antioxidant capacity, since it is in the *para* position to the carbonyl of the cyclic lactone, facilitating the transfer of the hydrogen atom to the oxygen-centered radical. Likewise, the presence of a catechol in the phenyl ring at position 3 of the coumarin increases the antioxidant capacity, while electron donor groups as methyl, or the absence of substituents in the coumarin, decrease the antioxidant capacity.

To corroborate the results of the antioxidant capacity, the radical Fukui indices (f_k^0), related to the attack mediated by radicals, were determined.

Table 3 Trypanocidal effect on trypomastigote of *T. cruzi* Dm28 and cytotoxicity on Vero cells by 3-arylcoumarins 1–11 at 100 μM .

| Compound | <i>T. cruzi</i> (%) | Vero cells at (%) |
|----------|---------------------|-------------------|
| 1 | 17.0 \pm 8.5 | 15.4 \pm 5.0 |
| 2 | 37.3 \pm 6.6 | 21.7 \pm 3.1 |
| 3 | 29.5 \pm 6.6 | 13.5 \pm 4.1 |
| 4 | 28.1 \pm 7.1 | 0.3 \pm 3.5 |
| 5 | 21.5 \pm 7.5 | 0.5 \pm 2.3 |
| 6 | 36.5 \pm 1.5 | 16.5 \pm 6.5 |
| 7 | 11.0 \pm 4.2 | 18.9 \pm 0.8 |
| 8 | 39.4 \pm 3.8 | 19.5 \pm 7.4 |
| 9 | 7.9 \pm 6.0 | 30.4 \pm 4.4 |
| 10 | 19.5 \pm 2.1 | 28.9 \pm 2.8 |
| 11 | 18.4 \pm 3.3 | 25.5 \pm 2.2 |
| Control* | 0.0 \pm 1.1 | 0.0 \pm 5.0 |
| BZN | 67.1 \pm 2.3 | 1.0 \pm 1.0 |

*Control: just the vehicles without the drugs.

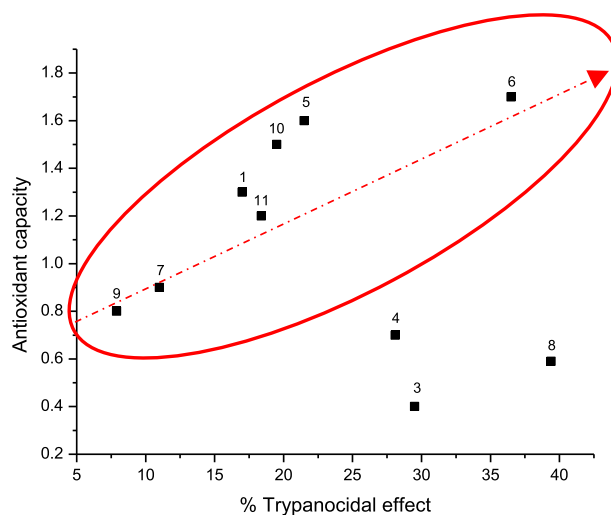
**Fig. 1** Interaction between the antioxidant capacity and the trypanocidal effect on the trypomastigotes of *T. cruzi* of 3-arylcoumarins 1–11.

Table 4 Determination of passive diffusion of the 3-aryl-coumarins 1–11 by PAMPA.

| Compound | Absorptivity coefficient (ϵ) ($\text{mM}^{-1}\cdot\text{cm}^{-1}$) | Diffused (%) | Retained (%) |
|-------------|--|-----------------|----------------|
| 1 | 5.0 | 0.90 \pm 0.08 | 89.7 \pm 1.0 |
| 2 | 12.2 | 23.6 \pm 3.9 | 29.2 \pm 4.1 |
| 3 | NS | NS | NS |
| 4 | NS | NS | NS |
| 5 | 5.6 | 0.12 \pm 0.05 | 44.0 \pm 1.0 |
| 6 | 19.8 | < LOD | 77.1 \pm 2.1 |
| 7 | 6.2 | 0.73 \pm 0.01 | 52.3 \pm 2.4 |
| 8 | 12.2 | < LOD | 78.8 \pm 0.8 |
| 9 | 2.3 | 0.94 \pm 0.09 | 49.1 \pm 0.9 |
| 10 | 5.7 | 0.6 \pm 0.1 | 59.0 \pm 1.2 |
| 11 | 5.0 | 0.5 \pm 0.1 | 39.6 \pm 2.9 |
| BZN | 6.0 | 37.7 \pm 0.1 | 42.5 \pm 0.3 |
| Evans blue* | 65.1 | < LOD | 49.6 \pm 5.2 |

NS: Not soluble in buffer, at pH 7.4. < LOD: below the detection limit. BZN: Benzimidazole * Evans blue is used as control, as it does not penetrate the artificial membrane.

3.3. Fukui indices

The Fukui indices allow evaluating the local reactivity of the oxygen atoms that participate in the reactions of the catechol groups from the studied series of compounds. The Fukui indices (Table 2) indicate that the catechol group has the highest reactivity, when included in the 3-aryl ring.

The f_k^0 values for all the compounds with the catechol group in the 3-aryl ring (O_3 and O_4) are similar. The radical attack occurs first in O_4 , since it is the most reactive atom (≈ -0.060). In compound 2, the presence of the hydroxyl group at position 6 of the coumarin leads to a decrease in the reactivity of the catechol group, being this hydroxyl group more prone to the radical attack, in accordance with what was previously described (Robledo-O’Ryan et al., 2017). Compounds 5 and 6 present a decrease in the reactivity of their catechol groups, similar to compound 2. Wherein, the reactivity of the hydroxyl groups (O_6 and O_7) is lower than compound 2, since both oxygens may interact with the oxygen of the carbonyl of the pyrone ring. Furthermore, the presence of halogens in compounds 7–9 does not affect the reactivity of the catechol groups, while the presence of a thiophenyl ring (compounds 9–11) decreases the reactivity of the catechol groups. The most probable site for a radical attack is carbon 4 (C_4), since the presence of a double bond would stabilize the free radical (Durand-Niconoff et al., 2016; Guíñez et al., 2013).

Based on the above, the antioxidant capacity of the coumarins under study depends significantly on the position of the isolated hydroxyl groups (and not the catechol), influenced by the substituent linked to the coumarin scaffold, having a direct relationship with the ORAC-FL values.

3.4. Trypanocidal activity and cytotoxicity in mammalian cells

The determination of the trypanocidal activity was carried out using the yellow tetrazolium salt (3-(4,5-dimethylthiazol-2-yl)-2,5-diphenyltetrazolium bromide) reduction methodology

(MTT, Table 3). 3-(3',4'-Dihydroxyphenyl)-6-hydroxycoumarin (2), 6,7-dihydroxy-3-(3'-hydroxyphenyl)coumarin (6) and 3-(3'-bromophenyl)-6,7-dihydroxycoumarin (8) showed the highest trypanocidal activities against *T. cruzi* trypomastigote within the studied series. These moderate activities may be influenced by the solubility, temperature, pH, among others (Hotez et al., 2012). Furthermore, the antioxidant capacity of the hydroxylated coumarins could also decrease the activity against this protozoan parasite.

The cytotoxicity of the compounds was also determined, using mammalian Vero cells (Table 3), proving 3-(3',4'-dihydroxyphenyl)-8-methylcoumarin (4) and 6,7-dihydroxy-3-(2'-hydroxyphenyl)coumarin (5) to be non-toxic at all. Compounds 2, 6, and 8, that showed the best trypanocidal activities, displayed the highest levels of toxicity as well.

Based on the experimental evidence, a possible trend between the antioxidant capacities and trypanocidal activities, was determined (Fig. 1). As observed in the chart, the increase in the antioxidant capacity is positively related with an increase in the trypanocidal effect (red circle and line). Compounds 3, 4 and 8 do not follow the observed trend, which could be due to the high lipophilicity comparing to the other compounds. In addition, a possible explanation is the difference in the mechanism of action of these compounds, i.e. involving the generation of oxidative stress, as described in previous studies (Moncada-Basualto et al., 2018).

3.5. Passive diffusion using the parallel permeability in the artificial membrane (PAMPA)

The determination of passive diffusion of the studied 3-arylcoumarins was carried out using the parallel artificial membrane permeability (PAMPA) assay. For this, a lipid monolayer formed by phosphatidylcholine in *n*-dodecane was used (Bujard et al., 2017). Table 4 shows the percentages of compounds retained and diffused on the artificial membrane.

The results show that most of the compounds were retained in a high percentage in the membrane. BZN has a lower percentage of retention, with a higher percentage of diffusion, comparing to the studied series. Compounds 6 and 8, that showed significant trypanocidal activities, were highly retained in the membrane, comparing to the other compounds, while compound 2 diffused in a higher proportion. This may indicate that the mechanism of action of 6 and 8 is different from 2. It is important to highlight that the PAMPA methodology is a preliminary test with short analysis times that allows identifying a possible passive diffusion of the compound through an artificial membrane, thus determining its physicochemical proper-

Table 5 IC₅₀ values in the trypomastigote form of *T. cruzi* Dm28 and Vero mammalian cells.

| Compound | <i>T. cruzi</i> (μM) | Vero cells (μM) | SI* |
|----------|--------------------------------------|---------------------------------|------|
| 2 | 186.2 \pm 0.6 | 177.8 \pm 0.3 | 0.9 |
| 6 | 185.1 \pm 0.4 | 192.3 \pm 0.3 | 1.0 |
| 8 | 33.6 \pm 0.7 | 162.2 \pm 0.3 | 4.8 |
| BZN | 20.0 \pm 0.5 | 321.6 \pm 0.5 | 16.8 |

* SI: Selectivity index; $SI = \frac{IC_{50} \text{ Vero cells}}{IC_{50} \text{ T. cruzi}}$

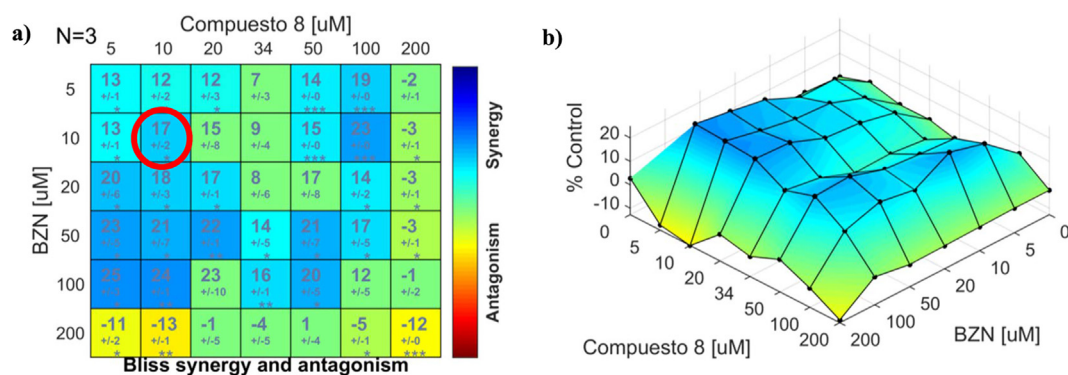


Fig. 2 a) Combination matrix of the actual data obtained for BZN and compound **8** using the independent Bliss model. b) Synergy heat map showing synergy for each combination. Combinations with statistical significance ($*p \leq 0.05$) are colored, and non-significant values are shown green. Data expressed as the mean of three independent experiments.

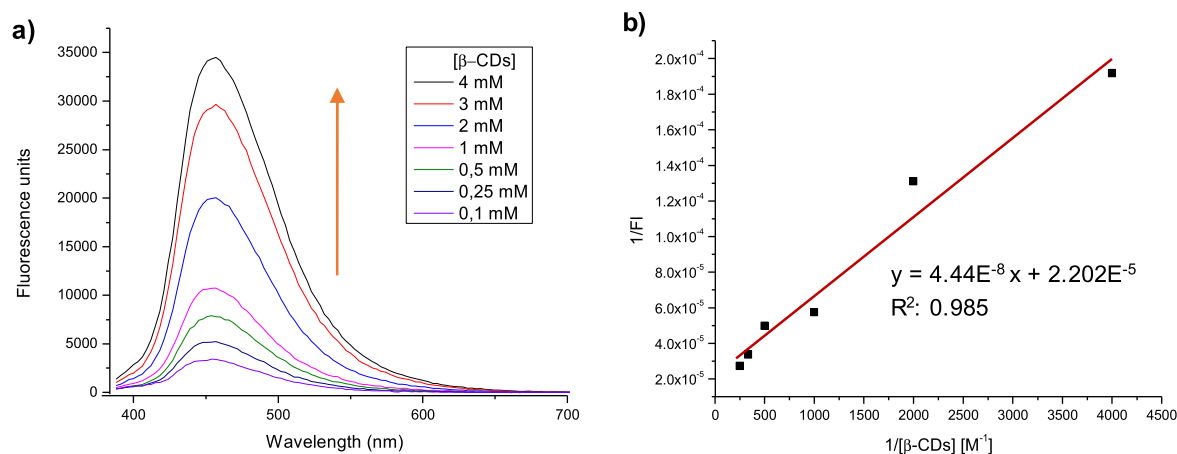


Fig. 3 a) Fluorescence spectrum of compound **8** with different concentrations of β -CDs, at 25 °C. b) Graphical representation of the Benesi-Hildebrand equation for the inclusion complex of compound **8** with β -CDs (**8**- β -CDs), at 25 °C.

ties. Therefore, to complement these results, it is necessary to work directly with the parasite and mammalian cells, since active transporters would help the diffusion of the compounds through the membrane (Miller and Dahan, 2012; Salgado et al., 2021). Therefore, the IC_{50} values on *T. cruzi* trypomastigotes and Vero cells were determined for the compounds that showed the highest trypanocidal activities (Table 5).

Compound **8** has a lower IC_{50} value than compounds **2** and **6**. On the other hand, it is the most toxic in mammalian cells, presenting a selectivity index (SI) of 4.8, less than BZN. When performing a structural analysis of compounds **2**, **6**, and **8**, all the three compounds have a catechol group in their structure, but in different positions. They also have an extra hydroxyl (compound **2** and **6**) or a bromine (compound **8**). In compound **2**, the catechol is found in the aryl substituent, while there is a hydroxyl group at position 6 of the coumarin scaffold. In the case of compounds **6** and **8**, the catechol is found at positions 6/7 of the coumarin, while in the aryl group for compound **6**, there is a hydroxyl group, and for compound **8**, a bromine. These two substituents are in *meta* position to the coumarin scaffold. For the future synthesis of compounds with higher trypanocidal activity, it is suggested to maintain

the basic structure of compound **8** and modify the halogen by functional groups or hydrocarbon chains with different lipophilicity.

3.6. Trypanocidal activity of compound **8** combined with BZN

A strategy used in the search for new treatments for diseases caused by protozoan parasites is combining traditional drugs with new bioactive compounds to enhance the therapeutic activity and reduce the adverse effects of conventional drugs (Castanheira et al., 2018; Seguel et al., 2016). The combination of antioxidants with BZN has been studied. During the acute phase of Chagas disease, there is a high proliferation of parasites and intense tissue inflammation, which exacerbates the generation of ROS/RNS (Goes et al., 2016; Hall et al., 2011). Furthermore, conventional drugs, BZN and NFX, being nitroheterocyclic compounds, also increase nitrosative and oxidative stress. This oxidative environment, associated with the intracellular multiplication of *T. cruzi*, leads to the destruction of host tissues, thus contributing to the etiopathogenesis of the disease.

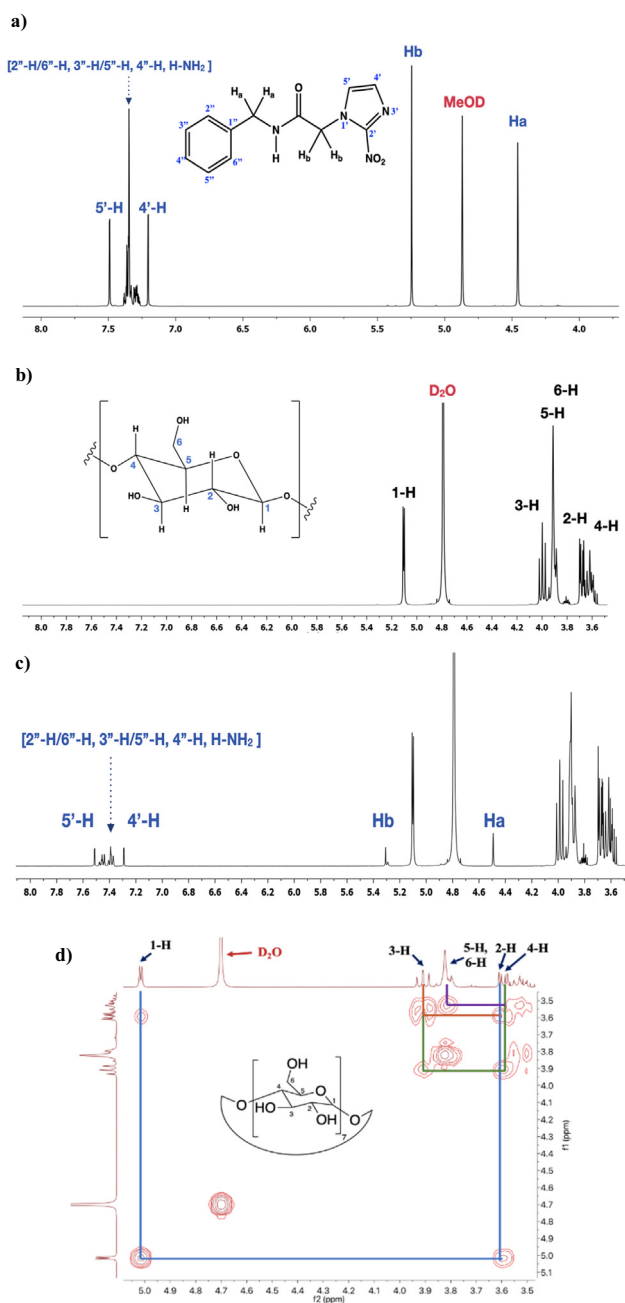


Fig. 4 NMR spectra of **a)** 1D ^1H of BZN, **b)** 1D ^1H of β -CDs, **c)** 1D ^1H of inclusion complex and **d)** 2D ^1H - ^1H COSY of β -CDs.

The combination was carried out using the most active compound of the series under study –compound **8**– with BZN. Considering that the trypanocidal mechanism of BZN involves: 1) the covalent modification of macromolecules by the formation of cytotoxic metabolites such as glyoxal; 2) the increase in phagocytosis of *T. cruzi* by the host cells with the consequent production of cytokines, and 3) the inhibition of NADH-fumarate reductase in the parasite (Providello et al., 2018; Wilkinson et al., 2008). These mechanisms are also responsible for adverse effects in the host. Therefore, the possibility of reducing the dose of BZN, in combination with antioxidant compounds, such as the one proposed here, seems to be an attractive strategy in the search for the treatment of chronic patients.

To determine the trypanocidal activity of the combination of **8**-BZN, a dose-matrix analysis of the combination of 7 different concentrations was performed. Data analysis was carried out using the free Combenefit software, selecting the Bliss independence statistical approach, assuming that both drugs have a different mechanism of action (Di Veroli et al., 2016). The dose-matrix combination shows the pattern of the combination between **8** and BZN (Fig. 2). Synergy heat maps were obtained by comparing the data recorded for each combination point, showing a synergistic effect at low concentrations of **8** and high concentrations of BZN. Likewise, an antagonistic effect at high concentrations of BZN and **8**, was observed. The IC_{50} value for compound **8** is 34 μM , and for BZN, 20 μM . Therefore, it was determined that the best combination is obtained for a concentration of 10 μM of both compounds (red circle), since the IC_{50} concentration of each compound was reduced almost 50%, being ideal for minimizing the dose and the consequent side effects.

Additionally, the activity on Vero cells of the best combination was evaluated, finding no cytotoxic activity at the concentration used. In addition, the trypanocidal activity of the best combination was 23%, which is still less than ideally expected. This can be related to the low solubility of compound **8** in aqueous medium, or structural changes mediated by pH or even enzyme.

3.7. β -cyclodextrin inclusion complexes and inclusion constant

A strategy used to increase the solubility of the organic compounds, as well as increase their bioavailability, is the formation of inclusion complexes with cyclodextrins (CD). Compound **8** was selected to form the inclusion complex since it had the best trypanocidal activity within the studied series. Likewise, the drug BZN was included in a CD as well. The

Table 6 Determination of the inclusion constant and the percentage of compound included in β -CDs and HP- β -CDs.

| Compound | β -CDs inclusion constant (M^{-1}) | Percentage of compound included in β -CDs (%) | HP- β -CDs inclusion constant (M^{-1}) | Percentage of compound included in HP- β -CDs (%) |
|----------|---|---|---|---|
| 2 | – | – | 4210 \pm 1409 | 77 \pm 7 |
| 6 | 5500 \pm 707 | 80 \pm 4 | 20000 \pm 1000 | 94 \pm 4 |
| 8 | 625 \pm 177 | 63 \pm 1 | 1286 \pm 100 | 67 \pm 7 |
| BZN | 52 \pm 10 | 20 \pm 1 | – | – |

Table 7 Chemical shifts of BZN and compound **8** when complexed with β -CDs.

| Proton | BZN- β -CDs | | | Proton | 8- β -CDs | | |
|-------------------|--|--|----------------------------|--------|--|--|-------------------------|
| | BZN _{free} δ (ppm) <i>J</i> (Hz) | Complex δ (ppm) <i>J</i> (Hz) | 12 $\Delta\delta$ (ppm) | | Comp. 8 _{free} δ (ppm) <i>J</i> (Hz) | Complex δ (ppm) <i>J</i> (Hz) | 12 $\Delta\delta$ (ppm) |
| 4'-H | 7.20 1.20 | 7.29 1.20 | 0.029 0 | 2'-H | 7.92 | 8.11 | 0.19 |
| 5'-H | 7.49 1.20 | 7.51 1.20 | 0.02 0 | 4'-H | 7.71 – 7.73 8.5 | 7.94 8.5 | 0.23 |
| H _a | 4.46 | 4.49 | 0.03 | 5'-H | 7.55 – 7.57 8.5 | 7.72 – 7.74 8.5 | 0.17 |
| H _b | 5.25 | 5.31 | 0.06 | 6'-H | 7.36 – 7.39 | 7.49 – 7.51 | 0.13 |
| 2'-H | 7.35 | 7.39 | 0.04 | 4-H | 8.19 | 8.39 | 0.20 |
| 3'-H | 7.29 | 7.37 | 0.08 | 5-H | 7.07 | 7.38 | 0.31 |
| 4'-H | 7.33 | 7.40 | 0.07 | 8-H | 6.79 | 7.34 | 0.55 |
| 5'-H | 7.29 | 7.37 | 0.08 | | | | |
| 6'-H | 7.35 | 7.39 | 0.04 | | | | |
| H-NH ₂ | 7.36 | 7.40 | 0.04 | | | | |

inclusion complexes were prepared by adding increasing amounts of β -CDs, keeping the concentration of the compounds constant, in an aqueous medium (Folch-Cano et al., 2011). Fig. 3 shows the variation of the fluorescence intensity as a function of the CD concentration. Increasing in the intensity of fluorescence as the CD concentration increases, indicates the compound's inclusion in the complex.

In Table 6 are represented the constant inclusion values of the complexes, determined by the Benesi-Hildebrand equation (Abdel-Shafi and Al-Shihry, 2009; Benesi and Hildebrand, 1949). The percentages of compound included were obtained by the Lucas-Abellan equation (Lucas-Abellán et al., 2014). The inclusion constant of **8** proved to be higher than BZN. This may be due to the high solubility of BZN in the polar environment, avoiding the migration towards the interior of the CD, which agrees with Leonardi *et al.* published data (Leonardi et al., 2013). The presence of hydroxyl groups in compound **8** accentuates polar characteristics. So, when using a derivative of β -CDs with polar characteristics such as hydroxypropyl β -CD (HP- β -CDs), the inclusion constant increased (Table 6), since the modification of the CD expands the cavity, which the hydroxypropyl groups generate. Therefore, it could keep the molecule included more effectively (C. Folch-Cano et al., 2010).

3.8. Inclusion geometry by NMR and molecular modeling

The determination of the inclusion geometry of BZN- β -CDs was carried out by 1D and 2D nuclear magnetic resonance (NMR). Fig. 4 shows the ¹H NMR spectrum of BZN, β -CDs, and the inclusion complex, as well as the characteristic signals for each. To corroborate the characteristic signals of the β -CDs, the two-dimensional COSY spectrum was recorded (Fig. 4). The signals from the BZN protons in the inclusion complex are shifted towards higher frequencies, probably due to interaction with CD. Table 7 shows that the difference in the chemical shifts of most signals is \sim 0.05–0.12 ppm, except for the aromatic protons multiplet of the benzyl fragment of BZN, which moved 0.02 ppm towards a higher frequency, which can be explained by the inclusion of the benzene ring in the β -CDs, generating interactions with the internal oxygen atoms of the

macrocycle, which confers an anisotropic protection region. On the other hand, the chemical shifts of greater magnitude can be explained by the interaction of the remaining protons of the BZN with the external oxygen atoms of the CDs, which exert a magnetic deprotection field that results in the displacement of the signals towards a lower field of the spectrum (Chadha et al., 2007).

For compound **8** (Fig. 5), the signals of the protons corresponding to the aryl group up to the proton of carbon 4 of the coumarin scaffold are found inside the cavity of the CD, since they have lower displacements than the protons 5 and 8 of coumarin, which are unprotected (Table 7).

The inclusion geometry was obtained by molecular modeling. The β -CD structure optimized for **8** indicates that the compound is within the CD cavity. Fig. 6 shows the minimum energy structure obtained for the inclusion complex by the modern GFN2-xTB semiempirical method (Bannwarth et al., 2019). The bromine substituent of the aryl ring is directed towards the primary hydroxyls of the CD cavity generating Van der Waals interactions type, the oxygen of the pyrone of the coumarin interacts with the secondary hydroxyls through hydrogen bonding interactions, while the catechol group is partly external to the CD, which is corroborated by ¹H NMR. In addition, studies of inclusion complexes in HP- β -CD of coumarin derivatives such as: quercetin and silibinin determined that the main interactions of the compounds within the cyclodextrin are Van der Waals interactions type, confirming what was previously proposed (Kellici et al., 2015; Kellici, et al., 2016). In conclusion, molecular modeling is an optimal tool for determining the inclusion geometry of this type of coumarins, without the need for advanced and high-cost instruments.

Subsequently, the trypanocidal activity of the inclusion complex of compound **8** in the β -CD was evaluated against the trypomastigote form of *T. cruzi*. The cytotoxicity activity against Vero cells was evaluated as well. The obtained values were $18.0 \pm 6.1\%$ and $18.2 \pm 3.3\%$, respectively. Thus, the decrease in trypanocidal activity could be due to the inclusion of the active fraction of the molecule in the CDs, which reaffirms that the active fraction of the molecule is the substituent. Likewise, studies determined that the decrease in the cytotoxic activity of the inclusion complexes could be explained by the controlled release, which allows the cell to generate some

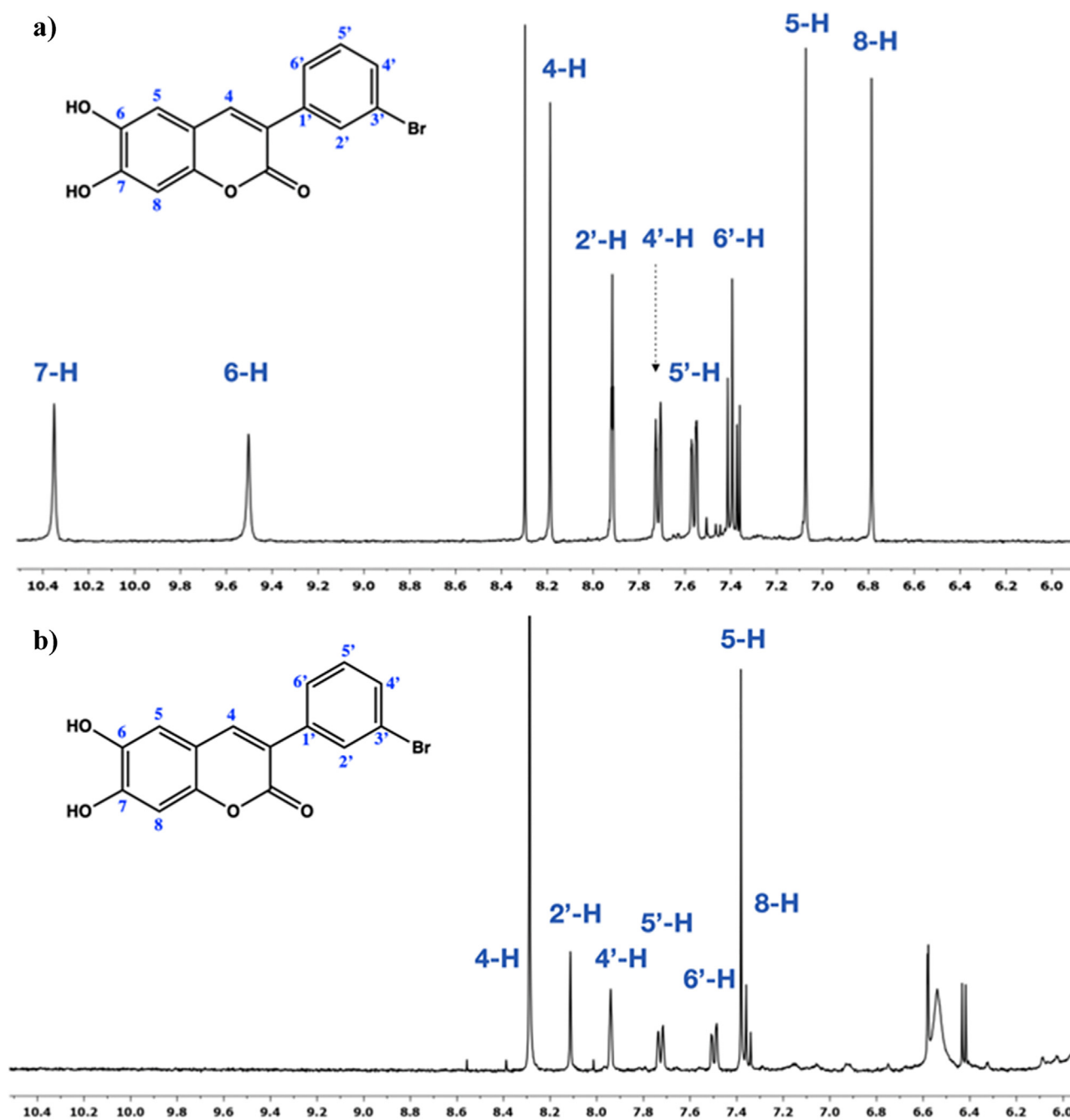


Fig. 5 NMR spectra of a) 1D ^1H of compound **8**, b) 1D ^1H of inclusion complex (**8**- β -CD).

defense mechanism (Lyra et al., 2012). The β -CD did not show trypanocidal activity.

Additionally, the passive diffusion of the inclusion complex was determined, finding that the percentage of compound retained in the membrane increased to 78.8%, and there were no changes in the percentage of diffusion. The increase in the retention percentage may be related to the increase in the compound's bioavailability (Moncada-Basualto et al., 2019; Paczkowska et al., 2018).

Several mechanisms have been described that can explain the increased permeability of coumarins when they form inclusion complexes, such as endocytosis, through transporters located in cell membranes and increased solubility (Moncada-Basualto et al., 2019; Réti-Nagy et al., 2015), the last one being a possible mechanism for compound **8** entrance into the cell when included in a β -CD. Being inside the cavity of the CD, it can be transported through the water layers that surround the cell unit to reach the cell membrane. Wherein, the

complex dissociates, and the free compound penetrates through the membrane.

The trypanocidal activity of the best combination (10:10 μM) was evaluated on the trypomastigote form of the parasite. The trypanocidal activity ($23 \pm 2\%$) increased comparing to the isolated compounds at the same concentration (**8**: $7 \pm 1\%$ and BZN: $1 \pm 1\%$), corroborating the synergism between the two compounds. In addition, the combination of compound **8** included in the CDs with BZN (**8**- β -CD-BZN) was evaluated, concluding that the trypanocidal effect ($25 \pm 4\%$) is higher than the non-included combination (**8**-BZN). This could be due to an increase in the solubility and bioavailability of the compound **8** when included in the CD. It should be highlighted that the combinations with the inclusion of BZN in CD were not evaluated, since having a low inclusion constant (k : $52 \pm 10 \mu\text{M}^{-1}$), a displacement of compound **8** towards the included BZN, generating the inclusion of **8**, may occur.

In addition, the cytotoxicity in mammalian cells of the combination of the compound **8** and **8** included in the CD with BZN, was evaluated, finding an increase in toxicity (**8**-BZN: $31 \pm 8\%$ and **8**- β -CD-BZN: $27 \pm 6\%$). This may be explained by a decrease in the defense mechanisms of the cells, counteracting the effects caused by the compound, being vulnerable to the other in the combination.

3.9. Intracellular trypanocidal activity of compound **8** and **8**-BZN

The trypanocidal effects of the free compounds and in combination on the intracellular amastigote form of *T. cruzi*, were evaluated. The Vero cells were previously infected with the parasite and incubated in the presence of the most active compound, the inclusion complex, and BZN, at the IC_{50} concentration. The combination with the drug BZN has a proportion of 10:10 μM , as described before.

Fig. 7 shows the images of the trypanocidal activities on the intracellular form of the *T. cruzi*, generated by the free compound **8**, included in the β -CD (**8**- β -CD) and in combination with BZN, obtained by fluorescence spectroscopy. Analyzing the data in Table 8, it is observed that the synergistic combination of BZN with compound **8** leads to a higher effect on Vero cells infection, than compound **8** and BZN alone, observing a decrease in the number of infected cells, but a slightly increase in the number of parasites per cell.

For **8**- β -CD, a decrease in the number of infected cells comparing to the free compound was observed, which may be attributed to the increase in the compound's bioavailability. Likewise, when comparing the combination of BZN with the inclusion complex of compound **8** (**8**- β -CD-BZN), a decrease in infected cells similar to that determined for the combination of free **8**, is observed, evidencing that there is no relevant difference between both combinations, attributable to the fact that the increase in the bioavailability of compound **8** does not imply an increase in the bioavailability of BZN, which seems to exert a higher effect on the infection of Vero cells, since it presents similar values as the drug *per se*.

However, it should be considered that the test considers the number of infected cells and the number of parasites per cell, and not the activity of the compounds on the intracellular amastigotes. Therefore, this test involves only the rate of infec-

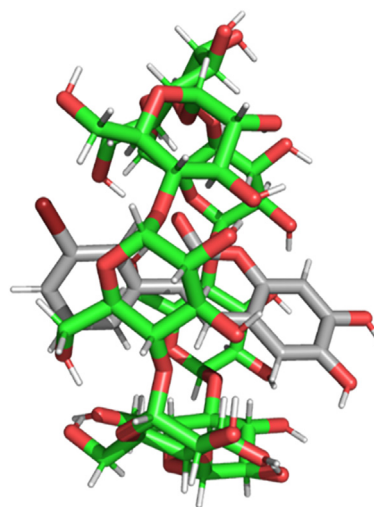


Fig. 6 The geometry of the inclusion complex of compound **8** in β -CDs, generating by molecular modeling.

tivity in mammalian cells after the treatment with the compound. In conclusion, all the compounds show an effect on the infection at the IC_{50} concentrations. In addition, the combination presents trypanocidal activity with a concentration lower than the free compounds. Therefore, the combined therapy becomes very important to reduce the dose of drug (Veas et al., 2020).

Based on the above, a study of the trypanocidal activity at 96 h of treatment was carried out, to evaluate the effect on the replication of the intracellular form (amastigote) and its differentiation to the trypomastigote form, in the presence of the compounds and the combinations of **8** and BZN, with or without CD inclusion. For this, the parasite DNA concentration was recorded using the real-time PCR (qPCR) technique. Furthermore, the same protocol of the intracellular study was followed, with the difference that at 96 h, the supernatant was removed and centrifuged at the precipitation rate of the trypomastigote form of *T. cruzi*, to quantify the parasite DNA.

Table 8 shows the number of parasites the managed to replicate, differentiate, and lyse the cells. BZN is the compound that presented the lowest number of parasites (750 ± 45), corroborating the result obtained in the intracellular trypanocidal activity study. This could be explained by the BZN damage to the amastigotes, preventing replication and subsequent differentiation. The same pattern was observed in the study of the intracellular trypanocidal effect, since the combination of **8** and the inclusion complex with BZN is better than compound **8** and BZN *per se*, corroborating the previous data. Based on the above, a study of the trypanocidal activity at 96 h of treatment was carried out, to evaluate the effect on the replication of the intracellular form (amastigote) and its differentiation to the trypomastigote form, in the presence of the compounds and the combinations of **8** and BZN, with or without CD inclusion. For this, the parasite DNA concentration was recorded using the real-time PCR (qPCR) technique. Furthermore, the same protocol of the intracellular study was followed, with the difference that at 96 h, the supernatant was removed and centrifuged at the precipitation rate of the trypomastigote form of *T. cruzi*, to quantify the parasite DNA.

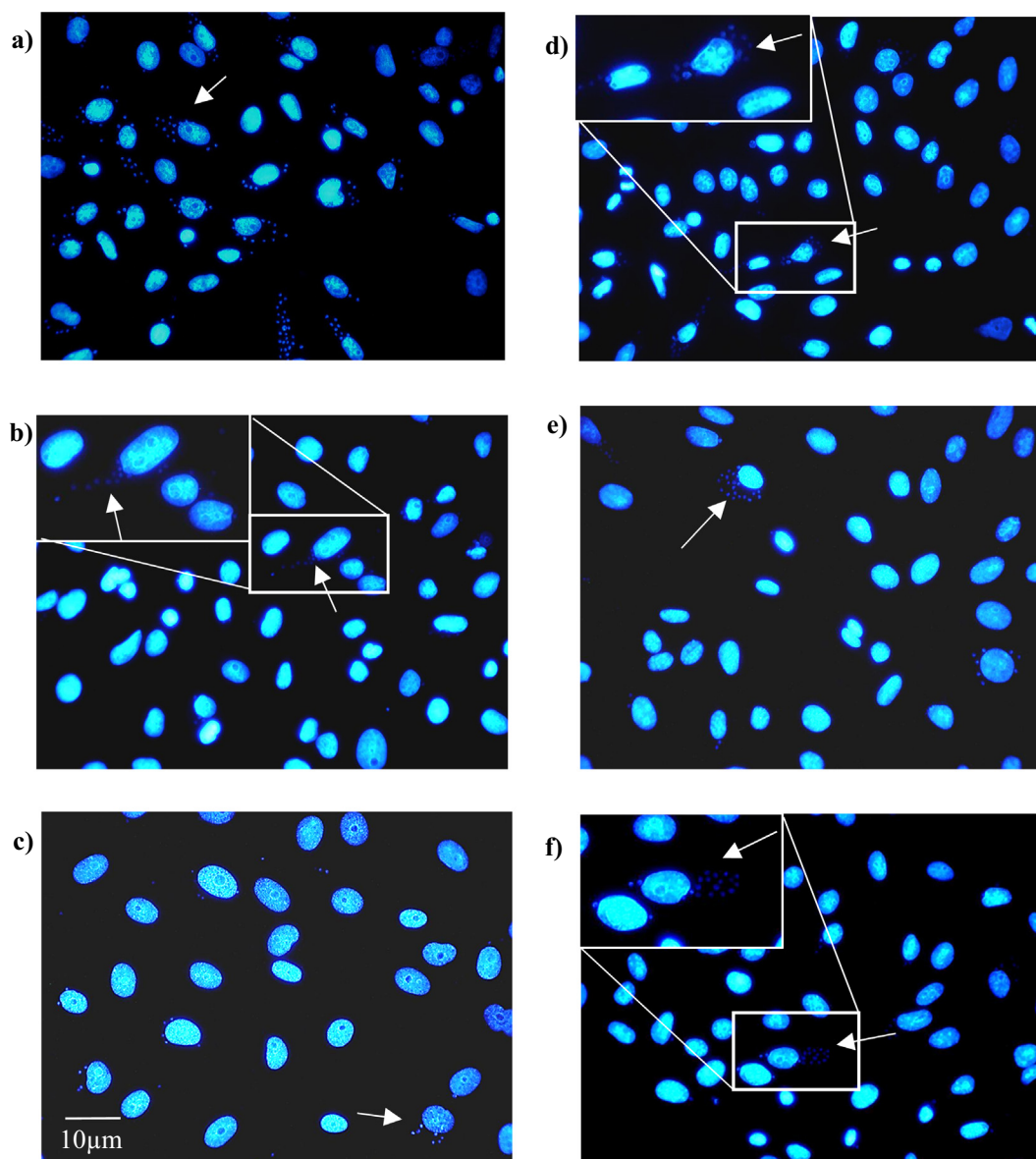


Fig. 7 Trypanocidal effect of **8** alone or combined with BZN on the amastigote forms of *T. cruzi*. Vero cells were exposed to a 1:3 ratio for 24 h, after which the supernatant was removed, and the cells were exposed to the compounds at the IC_{50} concentration, or the combination concentration, for 24 h. Each image is representative of **a**) Vero cells infected (control), **b**) BZN, **c**) compound **8**, **d**) 8- β -CD, **e**) 8-BZN and **f**) 8- β -CD-BZN. Arrows indicate the intracellular form of the parasite inside the Vero cell. The rows indicate the intracellular forms of *T. cruzi*.

Table 8 Determination of the trypanocidal effect and cytotoxicity of the best combination of **8** and BZN.

| Compound | Concentration (μ M) | % Not infected cells | % Infected cells | Parasite per cell | N° parasites post 96 h of treatment |
|--------------------|--------------------------|----------------------|------------------|-------------------|-------------------------------------|
| Control | – | 63 ± 7 | 40 ± 8 | 8 ± 2 | 157960 ± 1378 |
| BZN | 20 | 73 ± 5 | 30 ± 9 | 4 ± 1 | 750 ± 45 |
| 8 | 34 | 54 ± 7 | 51 ± 6 | 3 ± 1 | 50593 ± 2144 |
| 8- β -CD | 34 | 62 ± 5 | 40 ± 4 | 6 ± 1 | 150458 ± 1501 |
| 8-BZN | 10:10 | 77 ± 9 | 23 ± 6 | 5 ± 2 | 28999 ± 9700 |
| 8- β -CD-BZN | 10:10 | 80 ± 5 | 26 ± 8 | 4 ± 1 | 14559 ± 635 |

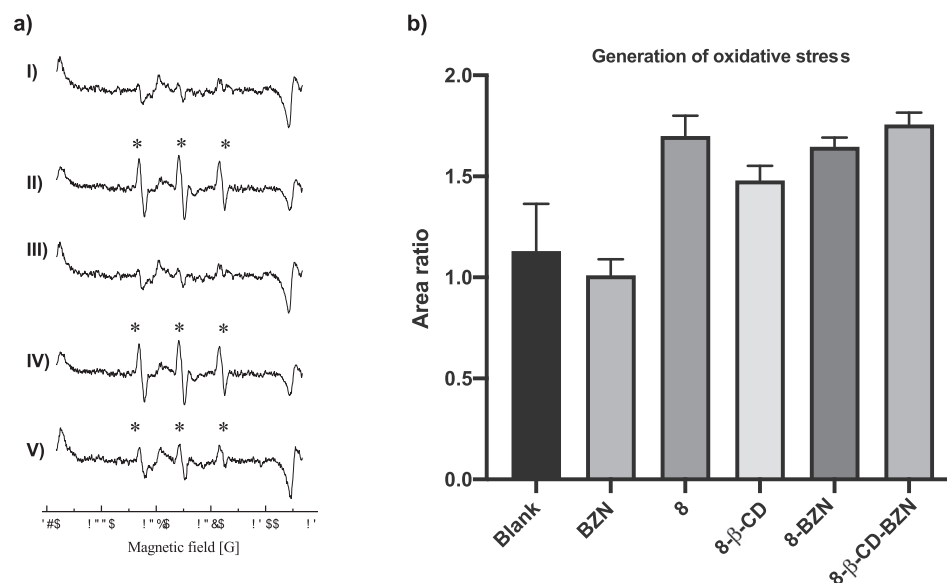


Fig. 8 a) EPR spectra of spin adducts generated on the trypanomastigote form of *T. cruzi* at room temperature. I) Spectrum recorded for the control, II) Spectrum recorded for compound **8**, III) Spectrum recorded for BZN, IV) Spectrum recorded for **8-BZN** and V) Spectrum recorded for compound **8-β-CD**, all incubated with trypanomastigotes. The DMPOX hyperfine pattern is represented by (*). b) Determination of the areas' ratios, for the compounds comparing to the blank.

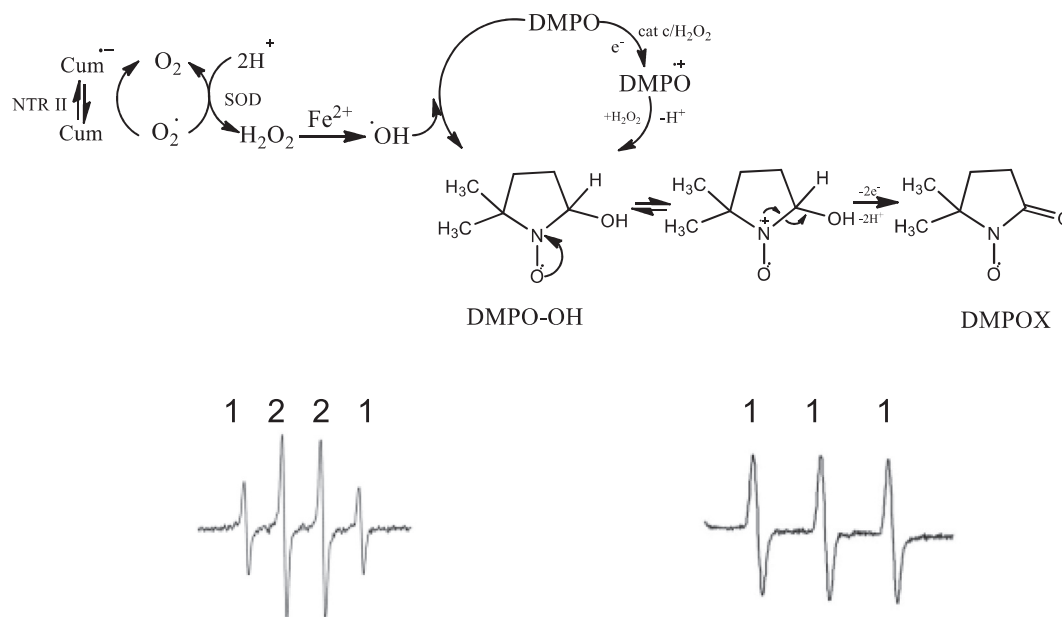


Fig. 9 Generation of radical species on the trypanomastigote form of *T. cruzi*, generation of metabolites and their interaction with the spin trapping DMPO.

3.10. Generation of radical species in a parasitic medium by electron spin resonance spectroscopy

Some coumarins have been reported to inhibit the enzyme GAPDH, an essential protein in the glycolytic pathway of trypanosomatids (Freitas et al., 2009). They can generate oxidative stress in the parasite, and deficit in the antioxidant mechanism (enzymatic and non-enzymatic) (Maria Aravena et al., 2011). Therefore, to understand the possible mechanism of action of the compound, the inclusion complex and the combination, the formation of radical species on the trypanomastigote form of *T. cruzi* was studied by electron spin resonance (ESR) spectroscopy.

The generation of radical species in cultures of trypanomastigote from *T. cruzi* was determined, using DMPO as a spin trap, since it does not generate radical species in a parasitic medium, it penetrates the cell membrane and reacts with free carbon and oxygen radicals (Barriga-González et al., 2015; Robledo-O’Ryan et al., 2017; Salgado et al., 2021). In Fig. 8a, hyperfine coupling patterns are observed. Compound **8**, **8-β-CD** and in combination with BZN, showed the same pattern, while BZN *per se* did not show any pattern. The hyperfine patterns represent the generation of

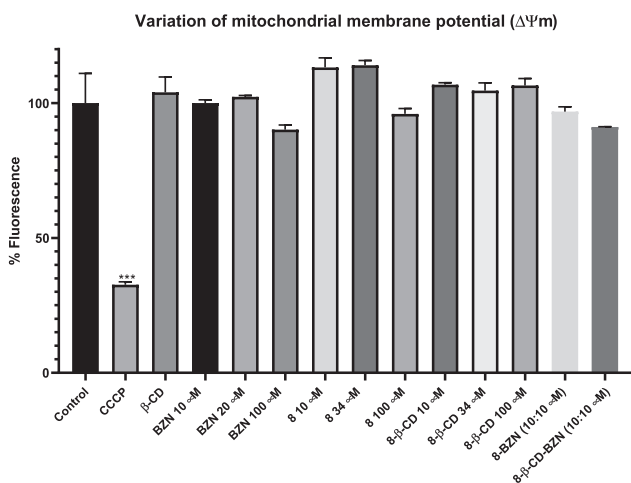


Fig. 10 Percentage of TMRM probe incorporation by variation of the mitochondrial membrane potential on trypomastigote of *T. cruzi*. The significant difference compared to control (one-way ANOVA with Dunnett's post-test, *** $p < 0.0001$).

a strong triplet signal with hyperfine coupling constants ($a_N \sim 14.62$ G), corresponding to the paramagnetic compound DMPOX (5,5-dimethyl-2-oxo-pyrrolin-1-oxyl), generated by the oxidation of the DMPO-OH adduct (Fig. 9). The calculation of the areas' ratio, comparing to the blank, allows determining that compound **8** and **8-β-CD** have area relations, like **8-β-CD-BZN**, while the **BZN** alone does not show any variation, which may indicate that it acts by a different mechanism of action.

The mitochondria of the *T. cruzi* parasite use oxidizable substrates to produce an electrochemical proton gradient across the mitochondrial membrane to produce ATP. Therefore, it would be very interesting to evaluate if the compounds may affect the mitochondrial membrane potential ($\Delta\Psi_m$). The *T. cruzi* parasite has only one mitochondrion, which is essential for survival, and regulates energy balance and apoptosis (Moncada-Basualto et al., 2019).

The mitochondrial metabolism has been assessed by varying the mitochondrial membrane potential. For this, the fluorescent tetramethylrhodamine methyl ester (TMRM) probe was used as an indicator of the potential variation. For the compound **8**, **8-β-CDs**, and **8-BZN**, no variations in the membrane potential were observed. Similarly, the **BZN** had no effect on the membrane potential, corroborating previous data (Hall et al., 2011). The decoupling agent carbonylcyanide-3-chlorophenylhydrazone (CCCP) was used as a control (Fig. 10).

Based on the results, it is postulated that the mechanism of action of compound **8** does not affect the mitochondrial membrane potential of the parasite. It can be associated with the generation of oxidative stress in *T. cruzi*, as previously demonstrated.

4. Conclusions

All the studied compounds display a moderate trypanocidal activity, being postulated that the mechanism of action is through the generation of oxidative stress, suggesting the

involvement of essential enzymes for the survival of the parasite. Also, membrane permeability studies indicate that trypanocidal activity is dependent on the lipophilicity. In addition, it was determined that the generation of β -CD inclusion complexes improves the bioavailability of the compounds, being a promising strategy for the administration of anti-chagasic drugs. Finally, the combination of different molecules proved to be an interesting approach for reducing the dose of conventional drugs that present severe side effects for the patient. Based on the results obtained, it would be interesting to further study a series of compounds that maintain the catechol group in different positions of the coumarin scaffold, since it may modulate the trypanocidal activity by generating oxidative stress. In addition, modifying the position and type of halogen (chlorine or fluorine) may decrease the cytotoxicity and increase the trypanocidal activity. Also, substituents that present electron withdrawing characteristics can be an alternative to study. Furthermore, the use of different CD, hydrogels, nanoparticles, among others, may increase the bioavailability of the compounds, and improve the trypanocidal activities.

Declaration of Competing Interest

The authors declare that they have no known competing financial interests or personal relationships that could have appeared to influence the work reported in this paper.

Acknowledgements

This project was partially supported by the FONDECYT (projects 1190340 and 1190341) and FONDECYT POSTDOC-TORADO 3190449. MJM thanks Xunta de Galicia (Galician Plan of Research, Innovation and Growth 2011–2015, Plan I2C, Grants ED481B 2014/086–0 and ED481B 2018/007) and Fundação para a Ciência e Tecnologia (FCT, CEECIND/02423/2018, UIDB/00081/2020 and PTDC/ASP-PES/28397/2017).

References

- Abdel-Shafi, A.A., Al-Shihry, S.S., 2009. Fluorescence enhancement of 1-naphthol-5-sulfonate by forming inclusion complex with β -cyclodextrin in aqueous solution. *Spectrochim. Acta Part A Mol. Biomol. Spectrosc.* 72 (3), 533–537.
- Ackermann, T. (1987). K. A. Connors: Binding constants — the measurement of molecular complex stability, John Wiley & Sons, New York, Chichester, Brisbane, Toronto, Singapore 1987. 411 Seiten, Preis: £ 64.15. *Berichte der Bunsengesellschaft für physikalische Chemie*, 91(12), 1398-1398.
- Balasubramani, S.G., Chen, G.P., Coriani, S., Diedenhofen, M., Frank, M.S., Franzke, Y.J., Yu, J.M., 2020. TURBOMOLE: Modular program suite for ab initio quantum-chemical and condensed-matter simulations. *J Chem Phys* 152, (18) 184107.
- Bannwarth, C., Caldeweyher, E., Ehlert, S., Hansen, A., Pracht, P., Seibert, J., Grimme, S., 2021. Extended tight-binding quantum chemistry methods. *WIREs Comput. Mol. Sci.* 11, (2) e1493.
- Bannwarth, C., Ehlert, S., Grimme, S., 2019. GFN2-xTB—An Accurate and Broadly Parametrized Self-Consistent Tight-Binding Quantum Chemical Method with Multipole Electrostatics and Density-Dependent Dispersion Contributions. *J. Chem. Theory Comput.* 15 (3), 1652–1671.

- Barriga-González, G., Olea-Azar, C., Zuñiga-López, M.C., Folch-Cano, C., Aguilera-Venegas, B., Porcal, W., Cerecetto, H., 2015. Spin trapping: an essential tool for the study of diseases caused by oxidative stress. *Curr Top Med Chem* 15 (5), 484–495.
- Benesi, H.A., Hildebrand, J.H., 1949. A Spectrophotometric Investigation of the Interaction of Iodine with Aromatic Hydrocarbons. *J. Am. Chem. Soc.* 71 (8), 2703–2707.
- Brandenburg, J.G., Bannwarth, C., Hansen, A., Grimme, S., 2018. B97-3c: A revised low-cost variant of the B97-D density functional method. *J Chem Phys* 148, (6) 064104.
- Bujard, A., Petit, C., Carrupt, P.-A., Rudaz, S., Schappler, J., 2017. HDM-PAMPA to predict gastrointestinal absorption, binding percentage, equilibrium and kinetics constants with human serum albumin and using 2 end-point measurements. *Eur. J. Pharm. Sci.* 97, 143–150.
- Castanheira, J., Castanho, R.E.P., Rocha Jr., H., Pagliari, C., Duarte, M.I.S., Therezo, A.L.S., Martins, L.P.A., 2018. Paradoxical effects of vitamin C in Chagas disease. *Parasitol Int* 67 (5), 547–555.
- Chadha, R., Jain, D.V.S., Aggarwal, A., Singh, S., Thakur, D., 2007. Binding constants of inclusion complexes of nitroimidazoles with β -cyclodextrins in the absence and presence of PVP. *Thermochim Acta* 459 (1), 111–115.
- Chatelain, E., 2014. Chagas Disease Drug Discovery: Toward a New Era. *J. Biomol. Screen.* 20 (1), 22–35.
- Chen, A., Liu, M., Dong, L., Sun, D., 2013. Study on the effect of solvent on the inclusion interaction of hydroxypropyl- β -cyclodextrin with three kinds of coumarins by phase solubility method. *Fluid Phase Equilib.* 341, 42–47.
- de Alcantara, F.C., Lozano, V.F., Vale Velosa, A.S., dos Santos, M.R.M., Pereira, R.M.S., 2015. New coumarin complexes of Zn, Cu, Ni and Fe with antiparasitic activity. *Polyhedron* 101, 165–170.
- Di Veroli, G.Y., Fornari, C., Wang, D., Mollard, S., Bramhall, J.L., Richards, F.M., Jodrell, D.I., 2016. CombeneFit: an interactive platform for the analysis and visualization of drug combinations. *Bioinformatics* 32 (18), 2866–2868.
- Duaso, J., Yanez, E., Castillo, C., Galanti, N., Cabrera, G., Corral, G., Kemmerling, U., 2012. Reorganization of extracellular matrix in placentas from women with asymptomatic chagas disease: mechanism of parasite invasion or local placental defense? *Journal of tropical medicine* 2012, 758357.
- Durand-Niconoff, J.S., Matus, M.H., Juárez-Cerrillo, S.F., Meléndez, F.J., 2016. Theoretical study of the global and local reactivity of a series of 3-aryl coumarins. *Theor. Chem. Acc.* 135 (11), 249.
- Eichkorn, K., Weigend, F., Treutler, O., Ahlrichs, R., 1997. Auxiliary basis sets for main row atoms and transition metals and their use to approximate Coulomb potentials. *Theor. Chem. Acc.* 97 (1), 119–124.
- Erk, C., Bulut, M., Göçen, A., 2000. The Synthesis of Novel Crown Ethers, Part VII [1]. Coumarin Derivatives of Benzocrowns and Cation Binding from Fluorescence Spectra. *J. Incl. Phenom. Macrocycl. Chem.* 37 (1), 441–450.
- Estani, S.S., Segura, E.L., 2017. Protozoan Diseases: Chagas Disease. In: Quah, S.R. (Ed.), *International Encyclopedia of Public Health*. Second Ed. Academic Press, Oxford, pp. 70–78.
- Fais, A., Era, B., Asthana, S., Sogos, V., Medda, R., Santana, L., Kumar, A., 2018. Coumarin derivatives as promising xanthine oxidase inhibitors. *Int. J. Biol. Macromol.* 120 (Pt A), 1286–1293.
- Folch-Cano, C., Jullian, C., Speisky, H., Olea-Azar, C., 2010. Antioxidant activity of inclusion complexes of tea catechins with β -cyclodextrins by ORAC assays. *Food Res. Int.* 43 (8), 2039–2044.
- Folch-Cano, C., Olea-Azar, C., Sobarzo-Sánchez, E., Alvarez-Lorenzo, C., Concheiro, A., Otero, F., Jullian, C., 2011. Inclusion Complex of 4-Hydroxycoumarin with Cyclodextrins and Its Characterization in Aqueous Solution. *J. Solution Chem.* 40 (11), 1835–1846.
- Forsyth, C.J., Hernandez, S., Olmedo, W., Abuhamidah, A., Traina, M.I., Sanchez, D.R., Meymandi, S.K., 2016. Safety Profile of Nifurtimox for Treatment of Chagas Disease in the United States. *Clin Infect. Dis.* 63 (8), 1056–1062.
- Freitas, R.F., Prokopczyk, I.M., Zottis, A., Oliva, G., Andricopulo, A. D., Trevisan, M.T.S., Montanari, C.A., 2009. Discovery of novel *Trypanosoma cruzi* glyceraldehyde-3-phosphate dehydrogenase inhibitors. *Bioorg. Med. Chem.* 17 (6), 2476–2482.
- Goes, G.R., Rocha, P.S., Diniz, A.R.S., Aguiar, P.H.N., Machado, C. R., Vieira, L.Q., 2016. *Trypanosoma cruzi* Needs a Signal Provided by Reactive Oxygen Species to Infect Macrophages. *PLoS Negl. Trop. Dis.* 10, (4) e0004555.
- Grimme, S., Antony, J., Ehrlich, S., Krieg, H., 2010. A consistent and accurate ab initio parametrization of density functional dispersion correction (DFT-D) for the 94 elements H-Pu. *J. Chem. Phys.* 132, (15) 154104.
- Grimme, S., Ehrlich, S., Goerigk, L., 2011. Effect of the damping function in dispersion corrected density functional theory. *J. Comput. Chem.* 32 (7), 1456–1465.
- Guíñez, R.F., Matos, M.J., Vazquez-Rodríguez, S., Santana, L., Uriarte, E., Olea-Azar, C., Maya, J.D., 2013. Synthesis and evaluation of antioxidant and trypanocidal properties of a selected series of coumarin derivatives. *Future Med. Chem.* 5 (16), 1911–1922.
- Hall, B.S., Bot, C., Wilkinson, S.R., 2011. Nifurtimox activation by trypanosomal type I nitroreductases generates cytotoxic nitrile metabolites. *J. Biol. Chem.* 286 (15), 13088–13095.
- Hotez, P.J., Dumonteil, E., Woc-Colburn, L., Serpa, J.A., Bezek, S., Edwards, M.S., Bottazzi, M.E., 2012. Chagas Disease: “The New HIV/AIDS of the Americas”. *PLoS Negl. Trop. Dis.* 6, (5) e1498.
- Jimenez, V., Kemmerling, U., Paredes, R., Maya, J.D., Sosa, M.A., Galanti, N., 2014. Natural sesquiterpene lactones induce programmed cell death in *Trypanosoma cruzi*: A new therapeutic target? *Phytomedicine* 21 (11), 1411–1418.
- Juvonen, R.O., Jokinen, E.M., Javai, A., Lehtonen, M., Raunio, H., Pentikäinen, O.T., 2020. Inhibition of human CYP1 enzymes by a classical inhibitor α -naphthoflavone and a novel inhibitor N-(3, 5-dichlorophenyl)cyclopropanecarboxamide: An in vitro and in silico study. *Chem. Biol. Drug Des.* 95 (5), 520–533.
- Kellici, F.T., Ntountaniotis, D., Leonis, G., Chatziathanasiadou, M., Chatzikonstantinou, V.A., Becker-Baldus, J., Glaubitz, C., Tzakos, G.A., Viras, K., Chatzigeorgiou, P., Tzimas, S., Kefala, E., Valsami, G., Archontaki, H., Papadopoulos, M., Mavromoustakos, T., 2015. Investigation of the interactions of Silibinin with 2-hydroxypropyl- β -cyclodextrin through biophysical techniques and computational methods. *Mol. Pharm.* 12 (3), 954–965.
- Kellici, F.T., Chatziathanasiadou, V.M., Diamantis, D., Chatzikonstantinou, V.A., Andreadelis, I., Christodoulou, E., Valsami, G., Mavromoustakos, T., Tzakos, G.A., 2016. Mapping the interactions and bioactivity of quercetin-(2-hydroxypropyl)- β -cyclodextrin complex. *Int. J. Pharm.* 511 (1), 303–311.
- Leonardi, D., Bombardiere, M.E., Salomon, C.J., 2013. Effects of benzimidazole:cyclodextrin complexes on the drug bioavailability upon oral administration to rats. *Int. J. Biol. Macromol.* 62, 543–548.
- Liempi, A., Castillo, C., Cerda, M., Droguett, D., Duaso, J., Barahona, K., Kemmerling, U., 2015. *Trypanosoma cruzi* infectivity assessment in “in vitro” culture systems by automated cell counting. *Acta Trop.* 143, 47–50.
- Lucas-Abellán, C., Guillén, I., Mercader-Ros, M.T., Serrano-Martínez, A., Núñez-Delgado, E., Gabaldón, J.A., 2014. Fluorimetric determination of sulphathiazole in honey by means the formation of CDs inclusion complexes. *Carbohydr. Polym.* 103, 87–93.
- Lyra, M.A.M., Soares-Sobrinho, J.L., Figueiredo, R.C.B.Q., Sandes, J.M., Lima, Á.A.N., Tenório, R.P., Rolim-Neto, P.J., 2012. Study of benzimidazole-cyclodextrin inclusion complexes, cytotoxicity and trypanocidal activity. *J. Incl. Phenom. Macrocycl. Chem.* 73 (1), 397–404.
- Maria Aravena, C., Claudio Olea, A., Cerecetto, H., González, M., Maya, J.D., Rodríguez-Becerra, J., 2011. Potent 5-nitrofurantoin

- derivatives inhibitors of *Trypanosoma cruzi* growth: Electrochemical, spectroscopic and biological studies. *Spectrochim. Acta Part A Mol. Biomol. Spectrosc.* 79 (2), 312–319.
- Matos, M.J., Pérez-Cruz, F., Vazquez-Rodriguez, S., Uriarte, E., Santana, L., Borges, F., Olea-Azar, C., 2013. Remarkable antioxidant properties of a series of hydroxy-3-aryl coumarins. *Bioorg. Med. Chem.* 21 (13), 3900–3906.
- Miller, J.M., Dahan, A., 2012. Predicting the solubility–permeability interplay when using cyclodextrins in solubility-enabling formulations: Model validation. *Int. J. Pharm.* 430 (1), 388–391.
- Moncada-Basualto, M., Lapier, M., Maya, J.D., Matsuhira, B., Olea-Azar, C., Delogu, G.L., Matos, M.J., 2018. Evaluation of Trypanocidal and Antioxidant Activities of a Selected Series of 3-amidocoumarins. *Med Chem* 14 (6), 573–584.
- Moncada-Basualto, M., Matsuhira, B., Mansilla, A., Lapier, M., Maya, J.D., Olea-Azar, C., 2019. Supramolecular hydrogels of β -cyclodextrin linked to calcium homopoly-L-gulonate for release of coumarins with trypanocidal activity. *Carbohydr. Polym.* 204, 170–181.
- Paczkowska, M., Mizera, M., Sałat, K., Furgala, A., Popik, P., Knapik-Kowalczyk, J., Cielecka-Piontek, J., 2018. Enhanced pharmacological efficacy of sumatriptan due to modification of its physicochemical properties by inclusion in selected cyclodextrins. *Sci. Rep.* 8 (1), 16184.
- Pelizzaro-Rocha, K.J., Tiunan, T.S., Izumi, E., Ueda-Nakamura, T., Filho, B.P.D., Nakamura, C.V., 2010. Synergistic effects of parthenolide and benzimidazole on *Trypanosoma cruzi*. *Phytomedicine* 18 (1), 36–39.
- Providello, M. V., Carneiro, Z. A., Portapilla, G. B., do Vale, G. T., Camargo, R. S., Tirapelli, C. R., & de Albuquerque, S. (2018). Benefits of Ascorbic Acid in Association with Low-Dose Benzimidazole in Treatment of Chagas Disease. *Antimicrobial Agents and Chemotherapy*, 62(9), e00514-00518.
- Pérez-Cruz, F., Villamena, F.A., Zapata-Torres, G., Das, A., Headley, C.A., Quezada, E., Olea-Azar, C., 2013. Selected hydroxy-coumarins as antioxidants in cells: physicochemical and reactive oxygen species scavenging studies. *J. Phys. Org. Chem.* 26 (10), 773–783.
- Pérez-Cruz, K., Moncada-Basualto, M., Morales-Valenzuela, J., Barriga-González, G., Navarrete-Encina, P., Núñez-Vergara, L., Olea-Azar, C., 2018. Synthesis and antioxidant study of new polyphenolic hybrid-coumarins. *Arabian J. Chem.* 11 (4), 525–537.
- Reed, A.E., Weinstock, R.B., Weinhold, F., 1985. Natural population analysis. *J. Chem. Phys.* 83 (2), 735–746.
- Robledo-O’Ryan, N., Matos, M.J., Vazquez-Rodriguez, S., Santana, L., Uriarte, E., Moncada-Basualto, M., Olea-Azar, C., 2017. Synthesis, antioxidant and antichagasic properties of a selected series of hydroxy-3-aryl coumarins. *Bioorg Med Chem* 25 (2), 621–632.
- Robledo-O’Ryan, N., Matos, M.J., Vazquez-Rodriguez, S., Santana, L., Uriarte, E., Moncada-Basualto, M., Olea-Azar, C., 2017. Synthesis, antioxidant and antichagasic properties of a selected series of hydroxy-3-aryl coumarins. *Bioorg. Med. Chem.* 25 (2), 621–632.
- Réti-Nagy, K., Malanga, M., Fenyvesi, É., Szente, L., Vámosi, G., Váradi, J., Fenyvesi, F., 2015. Endocytosis of fluorescent cyclodextrins by intestinal Caco-2 cells and its role in paclitaxel drug delivery. *Int. J. Pharm.* 496 (2), 509–517.
- Salgado, F., Moncada-Basualto, M., Pozo-Martínez, J., Liempi, A., Kemmerling, U., Maya, J.-D., Olea-Azar, C., 2021. Chemical and biological analysis of 4-acyloxy-3-nitrocoumarins as trypanocidal agents. *Arabian J. Chem.* 14, (3) 102975.
- Seguel, V., Castro, L., Reigada, C., Cortes, L., Diaz, M.V., Miranda, M.R., López-Muñoz, R., 2016. Pentamidine antagonizes the benzimidazole’s effect in vitro, and lacks of synergy in vivo: Implications about the polyamine transport as an anti-*Trypanosoma cruzi* target. *Exp. Parasitol.* 171, 23–32.
- Sierpe, R., Noyong, M., Simon, U., Aguayo, D., Huerta, J., Kogan, M.J., Yutronic, N., 2017. Construction of 6-thioguanine and 6-mercaptopurine carriers based on β -cyclodextrins and gold nanoparticles. *Carbohydr Polym* 177, 22–31.
- Souza, D.H.F., Garratt, R.C., Araújo, A.P.U., Guimarães, B.G., Jesus, W.D.P., Michels, P.A.M., Oliva, G., 1998. *Trypanosoma cruzi* glycosomal glyceraldehyde-3-phosphate dehydrogenase: structure, catalytic mechanism and targeted inhibitor design. *FEBS Lett.* 424 (3), 131–135.
- Tablet, C., Matei, I., Hillebrand, M., 2012. The determination of the stoichiometry of cyclodextrin inclusion complexes by spectral methods: possibilities and limitations. *Stoichiometry and Research-The Importance of Quantity in Biomedicine*, 47–76.
- Ulrich-Merzenich, G.S., 2014. Combination screening of synthetic drugs and plant derived natural products—Potential and challenges for drug development. *Synergy* 1 (1), 59–69.
- Veas, R., Rojas-Pirela, M., Castillo, C., Olea-Azar, C., Moncada, M., Ulloa, P., Kemmerling, U., 2020. Microalgae extracts: Potential anti-*Trypanosoma cruzi* agents? *Biomed. Pharmacother.* 127, 110178.
- Villalta, F., Kierszenbaum, F., 1982. Growth of isolated amastigotes of *Trypanosoma cruzi* in cell-free medium. *J. Protozool.* 29 (4), 570–576.
- Wilkinson, S.R., Taylor, M.C., Horn, D., Kelly, J.M., Cheeseman, I., 2008. A mechanism for cross-resistance to nifurtimox and benzimidazole in trypanosomes. *Proc. Natl. Acad. Sci. U S A* 105 (13), 5022–5027.